European Journal of Medicinal Chemistry 125 (2017) 1172–1192

Contents lists available at ScienceDirect

European Journal of Medicinal Chemistry

journal homepage: http://www.elsevier.com/locate/ejmech

Research paper

Discovery of benzimidazole derivatives as modulators of mitochondrial function: A potential treatment for Alzheimer's disease

TaeHun Kim [a, b, 1], Ha Yun Yang [a, d, 1], Beoung Gun Park [a], Seo Yun Jung [a], Jong-Hyun Park [a], Ki Duk Park [a, b], Sun-Joon Min [c], Jinsung Tae [d], Hyejin Yang [e], Suengmok Cho [e], Sung Jin Cho [f], Hyundong Song [g], Inhee Mook-Jung [g], Jiyoun Lee [h, **], Ae Nim Pae [a, b, *]

[a] Convergence Research Center for Diagnosis, Treatment and Care System of Dementia, Korea Institute of Science and Technology, PO Box 131, Cheongryang, Seoul 130-650, Republic of Korea
[b] Biological Chemistry, Korea University of Science and Technology, Yuseong-Gu, Daejon 305-350, Republic of Korea
[c] Department of Applied Chemistry, Hanyang University, Ansan, Gyeonggi-do 15888, Republic of Korea
[d] Department of Chemistry, Yonsei University, Seodaemun-gu, Seoul 120-749, Republic of Korea
[e] Korea Food Research Institute, Sungnam 463-746, Republic of Korea
[f] New Drug Development Center, Daegu-Gyeongbuk Medical Innovation Foundation, Daegu, Republic of Korea
[g] Department of Biochemistry and Biomedical Sciences, College of Medicine, Seoul National University, 103 Daehak-ro, Seoul 110-799, Jongno-gu, Republic of Korea
[h] Department of Global Medical Science, Sungshin University, Seoul 142-732, Republic of Korea

ARTICLE INFO

Article history:
Received 25 August 2016
Received in revised form
5 November 2016
Accepted 7 November 2016
Available online 9 November 2016

Keywords:
Translocator protein
TSPO
Mitochondrial permeability transition pore
Alzheimer's disease
Mitochondrial dysfunction
Aβ

ABSTRACT

In this study, we designed a library of compounds based on the structures of well-known ligands of the 18 kDa translocator protein (TSPO), one of the putative components of the mPTP. We performed diverse mitochondrial functional assays to assess their ability to restore cells from Aβ-induced toxicity in vitro and in vivo. Among tested compounds, compound **25** effectively improved cognitive function in animal models of AD. Given the excellent in vitro and in vivo activity and a favorable pharmacokinetic profile of compound **25**, we believe that it can serve as a promising lead compound for a potential treatment option for AD.

1. Introduction

Alzheimer's disease (AD) is a neurodegenerative disorder, known as the most common cause of dementia associated with impairments of cognitive functions and memory [1]. The mechanism of AD pathogenesis still remains largely unknown, however, amyloid-β (Aβ) is recognized as the major hallmark of AD [2,3]. Not only Aβ is the main component of the amyloid plaques found in AD patients, but many recent studies have found that high levels of cellular Aβ cause mitochondrial dysfunction [4,5]. Since mitochondria are responsible for a diverse array of cellular processes such as energy production, metabolism, and cell death, the aftermath of mitochondrial dysfunction in neuronal cells would be particularly devastating. Moreover, given the protective functions of mitochondria against oxidative stress and protein misfolding, mitochondrial dysfunction further aggravates and even accelerates the progression of AD [6]. It has been suggested that the accumulation of Aβ disrupts intracellular Ca^{2+} homeostasis [7] and results in apoptosis of neurons [8]. Furthermore, mitochondrial Aβ appears to interact with cyclophilin D (CypD) and promotes opening of the mitochondrial permeability transition pore (mPTP), a multimeric protein complex in the inner membrane of mitochondria [8,9]. Opening of the mPTP induces the depolarization of the

* Corresponding author. Convergence Research Center for Diagnosis, Treatment and Care System of Dementia, Korea Institute of Science and Technology, PO Box 131, Cheongryang, Seoul 130-650, Republic of Korea.
** Corresponding author.
E-mail addresses: jlee@sungshin.ac.kr (J. Lee), anpae@kist.re.kr (A.N. Pae).
[1] These authors contributed equally to this work.

http://dx.doi.org/10.1016/j.ejmech.2016.11.017
0223-5234/

mitochondrial membrane potentials ($\Delta\Psi_m$), which in turn allows for uncontrolled passage of cytosolic solutes, damaging mitochondrial structure. This structural damage leads to mitochondrial dysfunction, the consequences of which include the impairment of energy production, the initiation of cell death pathways, and the accumulation of neurotoxic proteins [9].

Prolonged opening of the mPTP has been observed in many diseases such as myocardial reperfusion injury [10], amyotrophic lateral sclerosis (ALS) [11,12], traumatic brain injury [13], and AD [14], therefore, many research efforts have focused on finding regulators of the mPTP [13,15,16]. However, considering that the complete structure of the mPTP has not been fully characterized, identifying specific regulators of the mPTP is a challenging task. According to several hypothetical models, the mPTP appears to contain at least four proteins [16,17]; CypD, a voltage-dependent anion channel (VDAC), the adenine nucleotide translocator (ANT), and the 18 kDa translocator protein (TSPO) [18,19]. It has been suggested that natural compounds such as cyclosporine A [20], sangliferin A [21], and bongkrekic acid [22] appear to bind these putative components of the mPTP, and regulate its opening. Several recent studies have identified small molecule modulators of the mPTP that can restore cellular viability from Aβ-induced mitochondrial dysfunctions [23,24].

The 18 kDa TSPO has been studied extensively due to its involvement in chronic inflammation and neurological disorders [25,26]. Although it was first introduced as peripheral benzodiazepine receptor (PBR), later it was found to be expressed throughout the whole body including the brain, therefore renamed as TSPO. Recent reports suggesting its regulatory roles in the mPTP opening have drawn renewed attention to TSPO as a novel therapeutic target for neurodegenerative diseases [25,27,28]. In spite of much interest, small molecule ligands of TSPO remain relatively scarce in literature, and only a few compounds with a benzodiazepine core have been developed to date for diagnostic imaging and therapeutic applications [29]. We believe that structurally diverse sets of compounds would facilitate the identification of novel ligands with desirable physicochemical properties, therefore, set out to design new compounds by employing ligand-based virtual screening. Based on the virtual screening results, we designed and synthesized a library of compounds containing a benzimidazole scaffold. Biological activity of the synthesized library was evaluated by determining the mitochondrial membrane potential, ATP production, and ROS generation in cells suffering Aβ induced mitochondrial dysfunction. In addition, we tested a few selected compounds in both acute and transgenic (Tg) mice models of AD to assess their effects on the cognitive impairment. We performed in vitro binding assays of the most active compound for TSPO to confirm its target-specific activity, and analyzed its binding interactions *via* molecular docking studies.

2. Results and discussion

2.1. Pharmacophore modeling and virtual screening

To design TSPO ligands with a novel scaffold, we first generated a common feature pharmacophore model based on the structures of the previously reported neuroprotective TSPO ligands. A ligand-based pharmacophore model was generated by commercially available pharmacophore generation program, Catalyst/HipHop. To generate common feature pharmacophore models, five representative TSPO ligands were collected from the Integrity® database of Prous, and were used as training set compounds: 2-(2-(4-fluorophenyl)-1*H*-indol-3-yl)-*N*,*N*-dihexylacetamide (FGIN-1-27, K_i for TSPO = 3.25 nM), *N*,*N*-dibutyl-2-(6,8-dichloro-2-(4-chlorophenyl)imidazo[1,2-*a*]pyridin-3-yl)acetamide (K_i for TSPO = 2.68 nM), *N*-(4-chloro-2-phenoxyphenyl)-*N*-(2-isopropoxybenzyl)acetamide (DAA1097, IC_{50} for TSPO = 0.92 nM), *N*-(2,5-dimethoxybenzyl)-*N*-(5-fluoro-2-phenoxyphenyl)acetamide (DAA1106, IC_{50} for TSPO = 1.6 nM), and *N*-(*sec*-butyl)-1-(2-chlorophenyl)-*N*-methylisoquinoline-3-carboxamide (PK-11195, IC_{50} for TSPO = 1.1 nM) [25]. From this set of compounds, two pharmacophore models (model 1 and 2) were generated by differing in ring aromatic and hydrophobic feature options. Model 1 consists of one hydrogen bond acceptor, one hydrophobic aromatic and four hydrophobic features, whereas model 2 includes six different common features: one hydrogen bond acceptor, two ring aromatic, and three hydrophobic features. Instead of the hydrophobic aromatic feature in model 1, the ring aromatic feature was varied in model 2 to cover the hydrophobic property and to introduce a planar or flexible ring aromatic substituent in the hit compounds. Based on these two pharmacophore models, our in-house library as well as commercial libraries from Asinex (AsinexGold, 229,398 compounds; AsinexPlatinum, 125,231 compounds, Asinex, Moscow, Russia, www.asinex.com) and ChemDiv (693,042 compounds, ChemDiv, Inc. California, USA, www.chemdiv.com) have been utilized for virtual screening. Through the BEST flexible search of the databases, 278 compounds (model 1: 172; model 2: 106) were selected by fit values (3.50 out of 6.00) from the two models. Among them, 22 compounds (**VS001**–**VS022**, Table S1) were manually selected based on fit values, structural diversity, and the presence of essential functionality. All the selected compounds (**VS001**–**VS022**) share a common bicyclic core ring: 3*H*-imidazo[4,5-*c*]pyridine (**VS001**–**VS007**), 1*H*-benzo[*d*]imidazole (**VS008**–**VS010**), and 1*H*-imidazo[4,5-*b*]pyridine (**VS011**–**VS022**).

All 22 compounds were initially screened by mitochondrial functional assays including JC-1 assay and ATP production assay. Interestingly, three 1*H*-benzo[*d*]imidazole compounds (**VS008**–**VS010**) demonstrated excellent recovery of mitochondrial membrane potential (over 50% at 5 μM) in the JC-1 assay (see supplementary material, Table S1). Moreover, compound **VS008** showed suitable mapping with the built pharmacophore model (model 2) which is illustrated in Fig. 1A. Compounds **VS008**–**VS010** were further screened by the ATP production assay. **VS008** again showed moderate recovery of ATP production (20% at 5 μM) in Aβ treated cells, while **VS009** and **VS010** did not appear to affect ATP production. Therefore, we decided to focus on **VS008** as our lead compound **1** (Fig. 1B).

2.2. Chemistry

Based on the structure of compound **1**, we designed a library of benzimidazole derivatives, compounds **10**–**32**, which contained various functional groups corresponding to the common feature pharmacophore model (Fig. 1B). After performing preliminary mitochondrial functional assays with compounds **1** and **10**–**32**, we modified the existing scaffold to have diverse hydrophobic groups (**36**–**44**) as well as an additional hydrogen bond donor (**51**–**53**).

The benzimidazole derivatives **10**–**32** were synthesized by following the pathway described in Scheme 1. Substituted *N*-(2-iodophenyl)amide compounds **4a**–**f** were prepared *via* nucleophilic addition-elimination of the 2-iodoaniline **2** to aryl-substituted acyl chlorides **3a**–**f**. Compounds **4a**–**f** were then converted to the corresponding benzimidazole analogues **7a**–**f** *via* Ullmann-type condensation reaction in moderate yields ranging 40 to 60%. On the other hand, compounds **7g** and **7h** were obtained *via* an intramolecular cyclization of compounds **5a**–**b** with 2-(2,6-dichlorophenyl)acetic acid **6** in the presence of polyphosphoric acid (PPA) [30]. The *N*-alkylation of compounds **7a**–**h** with methyl 2-bromoacetate generated compounds **8a**–**h**, and the subsequent

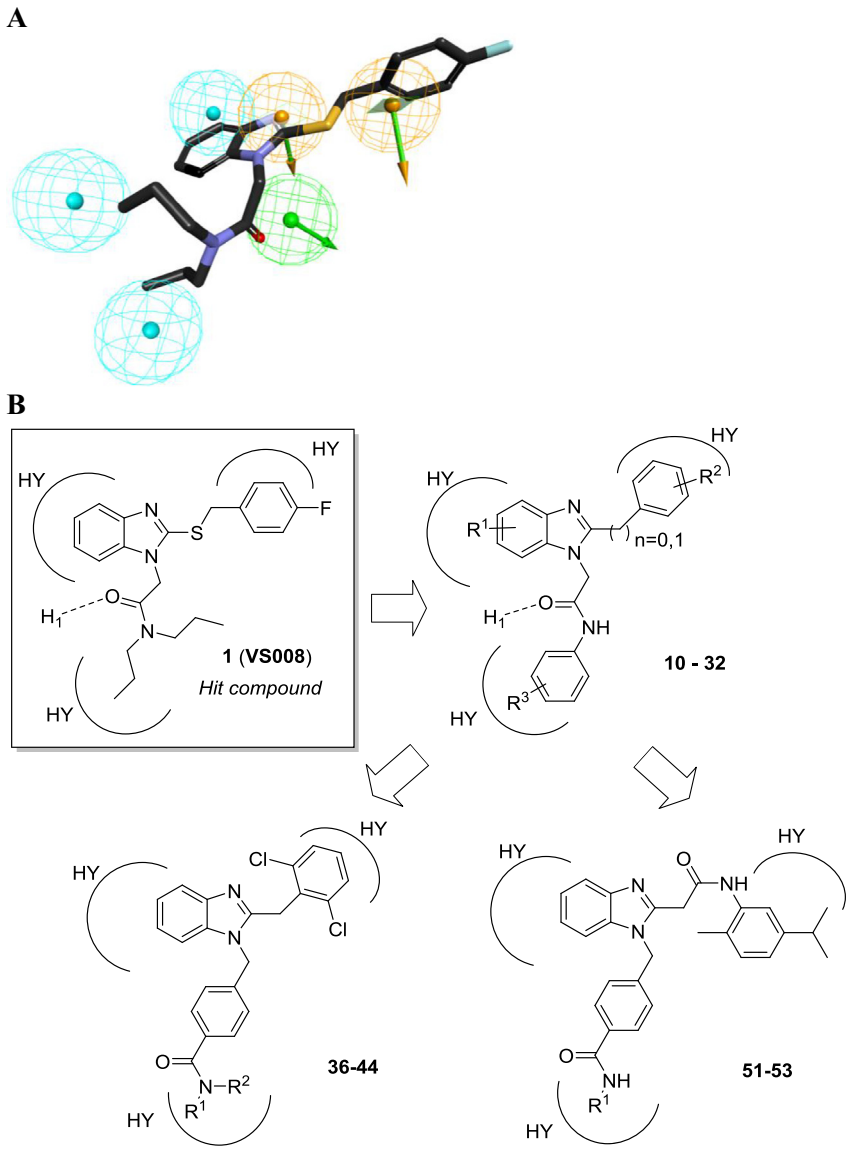

Fig. 1. Design of novel benzimidazole derivatives from hit compound **1** (**VS008**). (**A**) Compound **1** was mapped to the common feature pharmacophore model generated from representative TSPO ligands (Oxygen atom in red; nitrogen atom in blue; sulfur atom in yellow; fluoride atom in cyan; hydrophobic features in a cyan sphere; hydrophobic ring features in a yellow sphere with a vector; and hydrogen bond feature in a light green sphere with a vector). (**B**) Newly designed scaffolds of TSPO ligands (HY; Hydrophobic group, H_1; H-bond donor group). (For interpretation of the references to colour in this figure legend, the reader is referred to the web version of this article.)

hydrolysis followed by a peptide coupling reaction with substituted anilines led to the desired compounds **10**–**32**.

Compounds **36**–**44** were prepared from compound **7g** as shown in Scheme 2. The *N*-alkylation of **7g** by using methyl 4-(bromomethyl)benzoate **33** yielded compound **34**. Compound **34** was then hydrolyzed to carboxylic acid **35**, which was subjected to a peptide coupling reaction with *N*-substituted amines to generate 2-(2,6-dichlorobenzyl)-1*H*-benzo[*d*]imidazole derivatives **36**–**44**. Notably, the R^1 position of the *N*-substituted amines contains a diverse set of cycloalkylamines, which correspond to a hydrophobic feature in the pharmacophore model.

Compounds **51**–**53** were synthesized from commercially available 2-(1*H*-benzo[*d*]imidazol-2-yl)acetonitrile **45** as described in Scheme 3. The cyano group of **45** was hydrolyzed by 4 M NaOH to afford the carboxylic acid compound **46**. The subsequent peptide coupling reaction with 5-isopropyl-2-methylaniline **47** yielded compound **48**, which was further *N*-alkylated with methyl 4-(bromomethyl)benzoate **33** to generate compound **49**. Finally, the hydrolysis of **49**, followed by a peptide coupling reaction with alkyl amines led to the desired compounds **51**–**53**.

2.3. Effects on mitochondrial membrane potential

The electrochemical proton gradient across the mitochondrial membrane is the driving force of electron transport chain and essential for cellular respiration and energy production. This proton gradient is tightly regulated by double layers of mitochondrial membranes, and depolarization of the membrane potential is considered to be one of the first signs of mPTP opening. Therefore, to evaluate effects of the synthesized compounds on Aβ-induced mPTP opening, we used the ratiometric fluorescent dye JC-1 (5,59,6,69-tetrachloro-1,19,3,39-tetraethylbenz-imidazolocarbocyanine iodide), since the mitochondrial uptake of JC-1 is dependent on mitochondrial membrane potential ($\Delta\Psi_m$). JC-1 taken up by mitochondria forms red fluorescent J-aggregates, whereas cytoplasmic JC-1 emits green fluorescent light, hence,

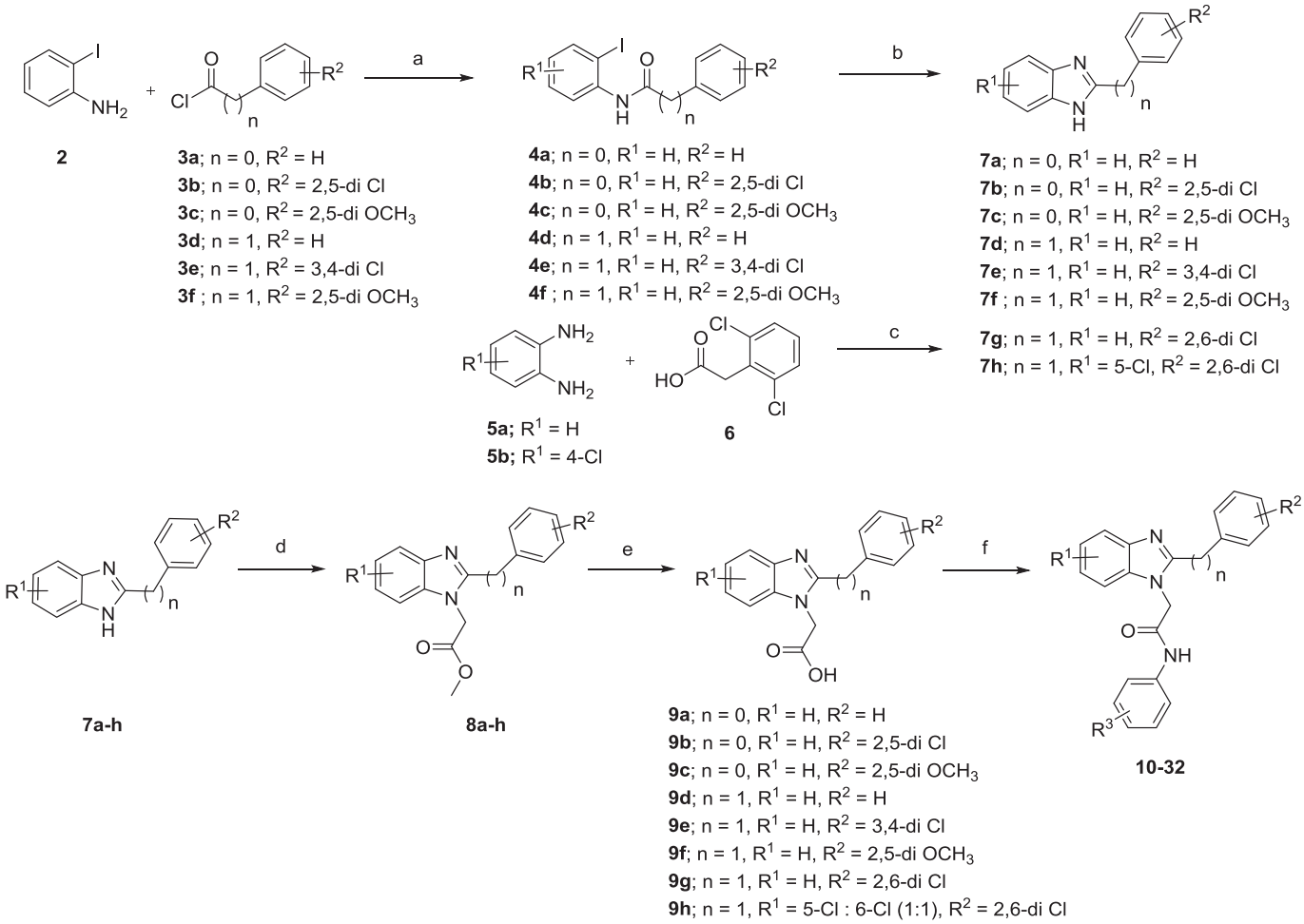

Scheme 1. Synthesis of benzimidazole derivatives **10**–**32**.[a]

[a] Reagents and conditions: (a) THF, r.t., 12–16 h, 63–87%, (b) (i) 30% NH_4OH, CuI, L-Proline, NaOH, DMSO, r.t., 1–2 h, (ii) AcOH, 80 °C, 6–7 h, 40–77%, (c) PPA, 180 °C, 4 h, 92%, (d) methyl 2-bromoacetate, NaH, DMF, r.t., 16 h, 39–95%, (e) 1 N NaOH, MeOH, r.t., 1–2 h, 70–95%, (f) aniline, HATU, Et_3N, MeCN, r.t., 16 h, 33–95%.

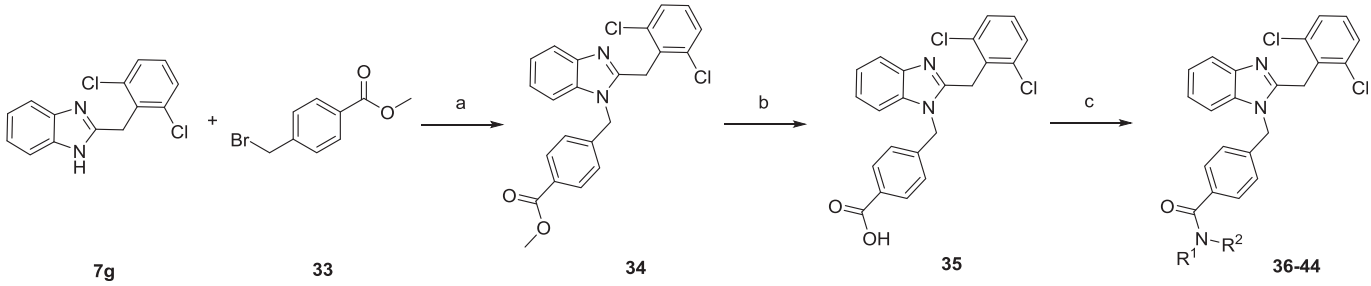

Scheme 2. Synthesis of 2-(2,6-dichlorobenzyl)-1*H*-benzo[*d*]imidazole Derivatives **36**–**44**.[a]

[a] Reagents and conditions: (a) NaH, DMF, r.t., 16 h, 52%, (b) LiOH, THF/MeOH, H_2O, r.t., 3 h, 53%, (c) (i) Oxalyl chloride, cat. DMF, CH_2Cl_2, 2 h, (ii) *N*-substituted amines, DIPEA, THF, r.t., 16 h, 37–79%.

mitochondrial membrane depolarization can be determined by a decrease in the red/green fluorescence intensity ratio. To measure the effects of each compound on $\Delta\Psi_m$, first, we treated a mouse hippocampal cell line, HT22 cells, with 5 μM of Aβ, subsequently incubated with 5 μM of each compound, and performed the JC-1 assay. Based on the changes of the red/green fluorescence intensity ratio between normal cells and Aβ-treated cells, we calculated percent recovery of $\Delta\Psi_m$ for each compound. For example, if the measured ratio of a compound treated sample is identical with normal cells, the percent recovery value for this particular compound should be 100%. We also included known neuroprotective compounds, piracetam and cyclosporine A (CsA) for comparison, since both compounds have been reported to exert their protective effects by restoring mitochondrial function [31,32] or blocking mPTP opening [17], respectively.

Initially, we measured the percent recovery values of $\Delta\Psi_m$ for compounds **10**–**32**, and these results are shown in Table 1. Compounds in this series mostly retained $\Delta\Psi_m$ to some extent.

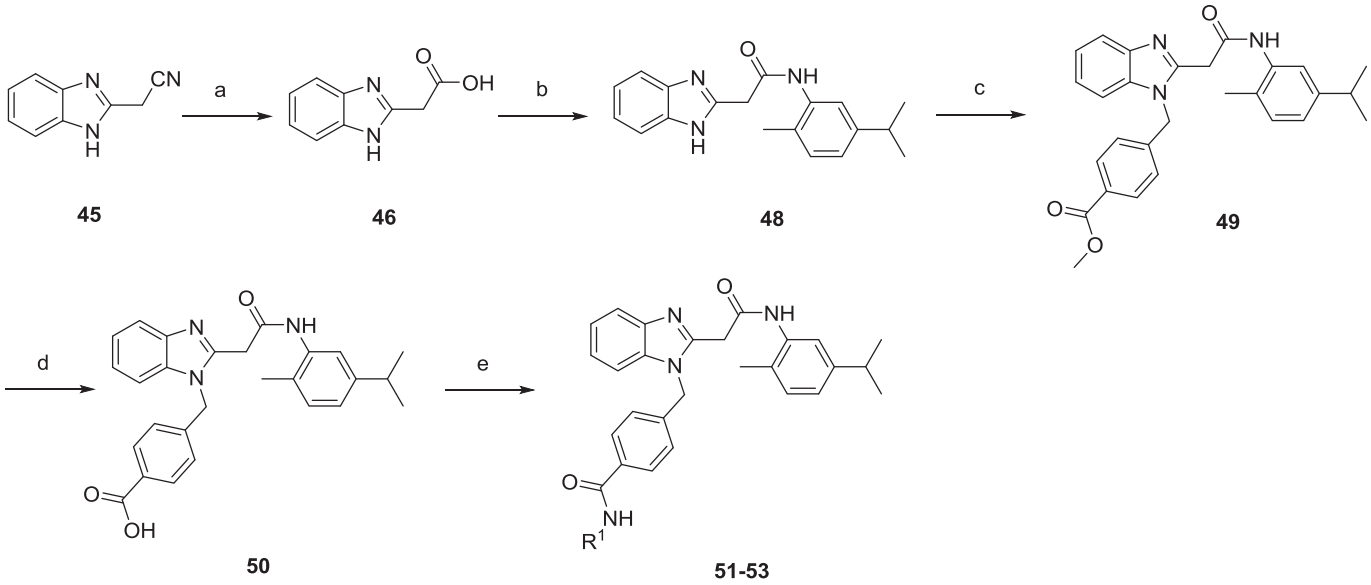

Scheme 3. Synthesis of 2-(1*H*-benzo[*d*]imidazol-2-yl)-*N*-(5-isopropyl-2-methylphenyl) acetamide Derivatives **51**–**53**.[a]
[a] Reagents and conditions: (a) 4 M NaOH, EtOH, Reflux, 8 h, 62%, (b) 5-isopropyl-2-methylaniline **47**, HATU, Et_3N, DMF, r.t., 4 h, 81%, (c) methyl 4-(bromomethyl)benzoate **33**, DIPEA, DMF, 80 °C, 6 h, 90%, (d) LiOH, THF/MeOH, H_2O, r.t., 3 h, 80%, (e) *N*-substituted amines, BOP, Et_3N, DMF, r.t., 16 h, 37–79%.

Compounds **10**–**15** and **24**–**31** showed comparable or greater percent recovery values compared to piracetam (60%) and CsA (55%). Compounds without aryl-substituents on the benzimidazole core (R_1 = H; **14** and **15**) were shown to be more potent (91%) than Cl-substituted derivatives (R_1 = Cl; **29**–**32**). On the other hand, compounds with a 2,5-dichlorophenyl group at the R_2 position (R_2 = 2,5-diCl; **14** and **15**) demonstrated higher activity than compounds without substituents (R_2 = H; **11** and **12**). Compounds with a 2-methyl 5-isopropyl group at the R_3 position (compounds **11**, **14**, **25**, **27**, **29**, and **30**) demonstrated significantly higher percent recovery compared to the rest of the compounds. Based on these findings, we further modified the benzimidazole scaffold to contain a dichlorobenzyl group (compounds **36**–**44**), and a 2-methyl 5-isopropyl group at the 2-position (compounds **51**–**53**). To focus on determining structure-activity relationship of hydrophobic interaction mimicking groups, we decided to replace the *N*-phenylacetamide group with various *N*-alkylbenzamide groups as shown in Table 2.

Interestingly, compounds in this series showed generally higher percent recovery compared to piracetam (60% at 5 μM) as well as compounds **10**–**32**. Two notable structural changes in this series are the removal of a hydrogen bond acceptor, and the addition of an alkylamide group to the benzyl side chain of the benzimidazole core, both of which appear to be beneficial for recovering mitochondrial membrane potential. The presence of a relatively bulky alkylamide group at the R_1 position seem to contribute to the protective effects regardless of their chain length. While compounds **36**–**44** share the same dichloro-substituted (2,6-diCl) benzyl group at the 2 position of the benzimidazole core, compounds **36**, **41**, and **42** demonstrated remarkably high percent recovery values, 89–90% recovery of $\Delta\Psi_m$ at 5 μM. Compounds **51**–**53** showed comparable potency (68–80%) at the same concentrations, although the addition of an extra amide bond did not affect overall activity significantly.

2.4. Effects on mitochondrial ATP production

Based on the JC-1 assay results, we selected compounds with great percent recovery values (over 60%), and further evaluated their effects on mitochondrial ATP production. To determine the effects of each compound, we treated HT22 cells with 5 μM of Aβ and selected compounds in the same manner as described for the JC-1 assays, and measured the amount of ATP generated by a luciferase-based assay. Based on the changes of luminescence intensity between untreated control cells and Aβ-treated cells, we calculated percent recovery of ATP production for each compound as shown in Table 3. We also calculated cell viability by measuring luminescence intensity of compound-treated cells in the absence of Aβ. Interestingly, piracetam appeared to induce over-production of ATP (127%), whereas CsA inhibited ATP production (−46%). Although it is unclear whether there is a correlation between the effects on $\Delta\Psi_m$ and ATP production of each compound, seven compounds (**13**, **25**, **28**, **30**, **36**, **38**, and **41**) restored over 50% of ATP production. In particular, compounds **25**, **28**, and **38** recovered ATP production close to control cells (**25**, 95%; **28**, 94%; and **38**, 85%) while maintaining excellent cell viability (**25**, 109%; **28**, 81%; and **38**, 93%). On the basis of these findings, we decided to move forward with eight compounds (**13**, **25**, **26**, **28**, **30**, **36**, **38**, and **41**) for further testing.

2.5. Effects on cell viability and reactive oxygen species (ROS) generation

To determine the effects on cell viability, we tested eight selected compounds (**13**, **25**, **26**, **28**, **30**, **36**, **38**, and **41**) by using 3-(4,5-dimethylthiazol-2-yl)-2,5-diphenyltetrazolium bromide (MTT). Again, we treated HT22 cells with 5 μM of Aβ and each compound in the same manner as described in the previous section, and calculated percent inhibition values based on the changes of the signal intensity between untreated cells and Aβ-treated cells. We also measured cell viability upon the treatment of each compound in the absence of Aβ *via* the MTT assay as described in Table 4. Among tested compounds, compounds **25** and **26** inhibited 30% and 36% of cellular toxicity induced by the treatment of Aβ, which is comparable to the effects of piracetam (29%). Several other compounds (**13**, **28**, and **39**) also showed noticeable protective effects against Aβ induced toxicity. Surprisingly, compounds **30, 36** and **38** demonstrated high percent recovery values in both ATP generation and $\Delta\Psi_m$, however, they did not appear to inhibit Aβ induced cellular toxicity significantly, suggesting that these

Table 1
In vitro activity of compounds **10**–**32** against Aβ-induced dissipation of $\Delta\Psi_m$.

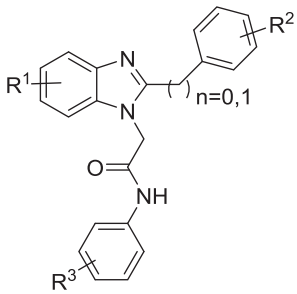

10 - 32

Compds	n	R^1	R^2	R^3	Recovery of $\Delta\Psi_m$ (%)[a]
1					57
10	0	H	H	3,5-di-*t*-Bu	86
11	0	H	H	2-Me-5-*i*Pr	63
12	0	H	H	3,5-diCl	69
13	0	H	H	2-*t*-Bu-6-Me	65
14	0	H	2,5-diCl	2-Me-5-*i*Pr	91
15	0	H	2,5-diCl	3,5-diCl	91
16	0	H	2,5-diCl	2-*t*-Bu-6-Me	41
17	0	H	2,5-diOMe	5-(Biphenyl-4-yloxy)-2-F	0
18	0	H	2,5-diOMe	2-Me-5-*i*Pr	41
19	1	H	H	3,5-di-*t*-Bu	29
20	1	H	H	2-Me-5-*i*Pr	24
21	1	H	H	5-(Biphenyl-4-yloxy)-2-F	0
22	1	H	H	2-*t*-Bu-6-Me	38
23	1	H	3,4-diCl	3,5-di-*t*-Bu	42
24	1	H	3,4-diCl	2-Me-5-*i*Pr	57
25	1	H	2,6-diCl	2-Me-5-*i*Pr	74
26	1	H	2,5-diOMe	3,5-di-*t*-Bu	54
27	1	H	2,5-diOMe	2-Me-5-*i*Pr	81
28	1	H	2,5-diOMe	3,5-diCl	68
29	0	5-Cl	2,5-diCl	2-Me-5-*i*Pr	60
30	0	6-Cl	2,5-diCl	2-Me-5-*i*Pr	87
31	0	5-Cl	2,5-diCl	3,5-diCl	77
32	0	6-Cl	2,5-diCl	3,5-diCl	18
CsA					55
Piracetam					60

[a] The increase of fluorescence ratio (green/red) after the treatment of each compound (5 μM) and Aβ (5 μM) in HT22 cell was normalized by dividing the difference of the ratio between 0% (Aβ-induced damaged condition) and 100% (normal condition in the absence of Aβ).

compounds may act on different pathways.

Next, we measured cellular ROS levels by using 2′,7′-dichlorofluorescein diacetate (DCFDA), a fluorescent indicator of cellular ROS. We measured fluorescence signal intensities and calculated percent inhibition of ROS generation based on the changes of the signal intensity between untreated cells and Aβ-treated cells. Piracetam and compounds **25** and **30** effectively reduced cellular ROS generated by the treatment of Aβ (piracetam: 129%, **25**: 85%, and **30**: 107%). Most of the tested compounds reduced cellular ROS levels to some extent, which generally corresponded to the results from MTT assays, except compounds **26** and **30**. Compound **26** demonstrated a relatively high recovery percent in the MTT assay (36%), however, it did not inhibit ROS generation significantly (10%). On the other hand, compound **30** did not recover cell death during the MTT assay (0%), while completely inhibited ROS generation (100%), suggesting this compound might act as a cellular antioxidant.

2.6. Effects on intracellular Ca^{2+} level

Opening of the mPTP allows sudden exchange of substances between mitochondria and cytosol, and also releases mitochondrial Ca^{2+} into cytosol resulting in the increased levels of intracellular Ca^{2+} [7]. It has been reported that the accumulation of Aβ induces mPTP opening, resulting in the increased intracellular Ca^{2+}, therefore, compounds that can inhibit mPTP opening maintain intracellular Ca^{2+} level within a normal range. We tested this hypothesis by measuring intracellular Ca^{2+} concentrations upon treating cells with a well-known TSPO ligand, **PK-11195** in the presence of 5 μM of Aβ. As shown in Fig. 2A, the treatment of Aβ at 5 μM increased intracellular Ca^{2+} concentrations up to 30%, while the treatment of **PK-11195** appeared to suppress opening of the mPTP in dose-dependent manner, demonstrating significantly reduced intracellular Ca^{2+} level compared to the Aβ treated control.

Next, based on the results from in vitro testings, we selected compound **25** ($\Delta\Psi_m$ recovery 74%, ATP recovery 95%, MTT assay 30%, and ROS inhibition 85%) to assess inhibitory effects against mPTP opening, and measured intracellular Ca^{2+} level. As shown in Fig. 2B, compound **25** suppressed mPTP opening in dose-dependent manner, exhibiting the reduced Ca^{2+} level even at the lowest concentration (0.1 μM). At 5 μM or higher concentrations, both **PK-11195** and compound **25** maintained the intracellular Ca^{2+} levels within a normal range.

2.7. CYP450 and hERG liability

Before we move forward to animal studies, we examined the toxicity profile of several selected compounds by measuring the

Table 2
In vitro activity of compounds **36**–**44** and **51**–**53** against Aβ-induced dissipation of $\Delta\Psi_m$.

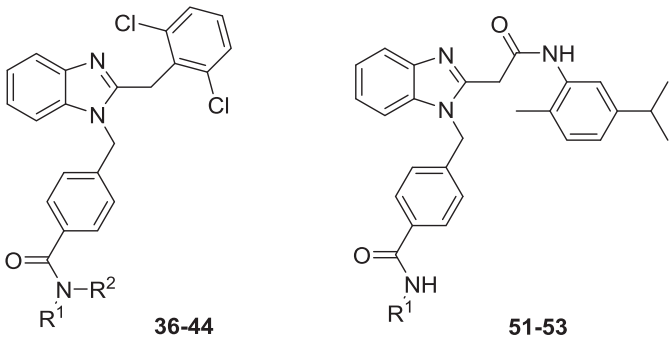

Compds	R^1	R^2	Recovery of $\Delta\Psi_m$ (%)[a]
36		H	90
37	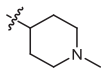	H	81
38	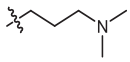	H	82
39	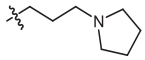	H	79
40	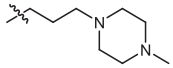	H	86
41	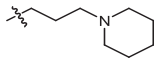	H	90
42	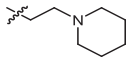	H	89
43	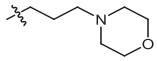	H	76
44	Me	Me	73
51		–	68
52	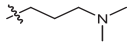	–	68
53	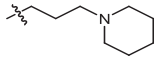	–	80
CsA			55
Piracetam			60

[a] The increase of fluorescence ratio (green/red) after the treatment of each compound (5 μM) and Aβ (5 μM) in HT22 cell was normalized by dividing the difference of the ratio between 0% (Aβ-induced damaged condition) and 100% (normal condition in the absence of Aβ).

inhibition of human ether-a-go-go-related gene (hERG) potassium channels and cytochrome P450 (CYP450) upon the treatment of each compound (Table 5). While all tested compounds appear to inhibit CYP450 to some extent, the treatment of compounds **25** and **38** affect overall activity of CYP450 less significantly, showing over 50% of remaining CYP450 activity for all five isoforms. Unfortunately, however, compounds **26** and **30** inhibited all tested isoforms of CYP450. As for the hERG channel related toxicity, compound **25** did not inhibit hERG channels, whereas compounds **26**, **36** and **38** inhibited hERG channels at a low micromolar range. Although compounds **26**, **30**, **36**, and **41** are potent inhibitors of mPTP opening in various cell-based assays, these compounds may exhibit moderate to high toxicity in vivo based on the inhibitory effects of CYP450 and hERG channels. Thus, we decided to continue further in vivo studies with compounds **25** and **38** in acute AD model mice.

2.8. Y-maze spontaneous alternation test

Based on the results from mitochondrial functional assays, we selected compounds **25** and **38** for further testings in acute AD model mice, which were prepared by injecting a 500 pmol of $A\beta_{1-42}$ i.c.v. by following the previously described method [33]. We administered compounds **25** and **38** by intraperitoneal injections for 6 days (30 mg/kg daily), and assessed spatial working memory of each mouse by performing Y-maze spontaneous alternation tests one day after the end of drug administration. We also included piracetam treated mice in parallel for comparison. The Y-maze test is a method to determine the willingness of rodents to explore new

Table 3
In vitro ATP production recovery Activities of the selected compounds.

Compds	ATP Production		Compds	ATP Production	
	Recovery[a]	Viability[b]		Recovery[a]	Viability[b]
10	4%	71%	**36**	51%	62%
11	19%	67%	**37**	8%	94%
13	55%	65%	**38**	85%	93%
14	0%	93%	**39**	31%	100%
15	0%	107%	**41**	64%	86%
25	95%	109%	**42**	4%	87%
26	46%	112%	**43**	1%	98%
27	0%	96%	**52**	14%	97%
28	94%	81%	**53**	23%	100%
29	3%	78%	**CsA**	−46%	82%
30	69%	86%	**Piracetam**	127%	88%

[a] Recovery of ATP production at 5 μM of each test compound against Aβ-induced mitochondrial ATP reduction.
[b] HT22 cell viability after the treatment with 5 μM of each compound only.

Table 5
CYP450 and hERG liability profiles of selected compounds.

Compds	CYP450 (% remaining Activity @ 10 μM)					hERG IC_{50} (μM)[a]
	CYP1A2	CYP2D6	CYP2C9	CYP3A4	CYP2C19	
25	107.60	140.41	54.69	223.73	57.30	>100
26	92.52	56.28	36.09	43.30	43.93	0.02 ± 0.02
30	56.29	82.23	29.65	15.43	11.89	ND[b]
36	62.97	82.36	50.58	130.27	31.43	1.57 ± 0.29
38	66.14	119.81	53.91	206.03	72.88	4.53 ± 1.50
41	68.41	25.49	61.08	176.46	67.28	ND[b]

[a] IC_{50} values (±SD) were obtained from a dose-response curve.
[b] Not determined.

memory. As shown in Fig. 3, both compounds **25** and **38** appear to restore cognitive function compared to vehicle control and piracetam administered mice. Compound **25** significantly improved

Table 4
In vitro MTT assay and ROS assay results.

Compds	MTT		ROS
	% Inhibition[a]	Viability[b]	% Inhibition[a]
13	16%	95%	0%
25	30%	88%	85%
26	36%	99%	10%
28	12%	82%	0%
30	0%	106%	107%
36	6%	122%	24%
38	7%	111%	9%
39	12%	101%	15%
41	3%	118%	27%
Piracetam	29%	132%	129%

[a] Against Aβ-induced toxicity at 5 μM.
[b] HT22 cell viability after the treatment with 5 μM of each compound only.

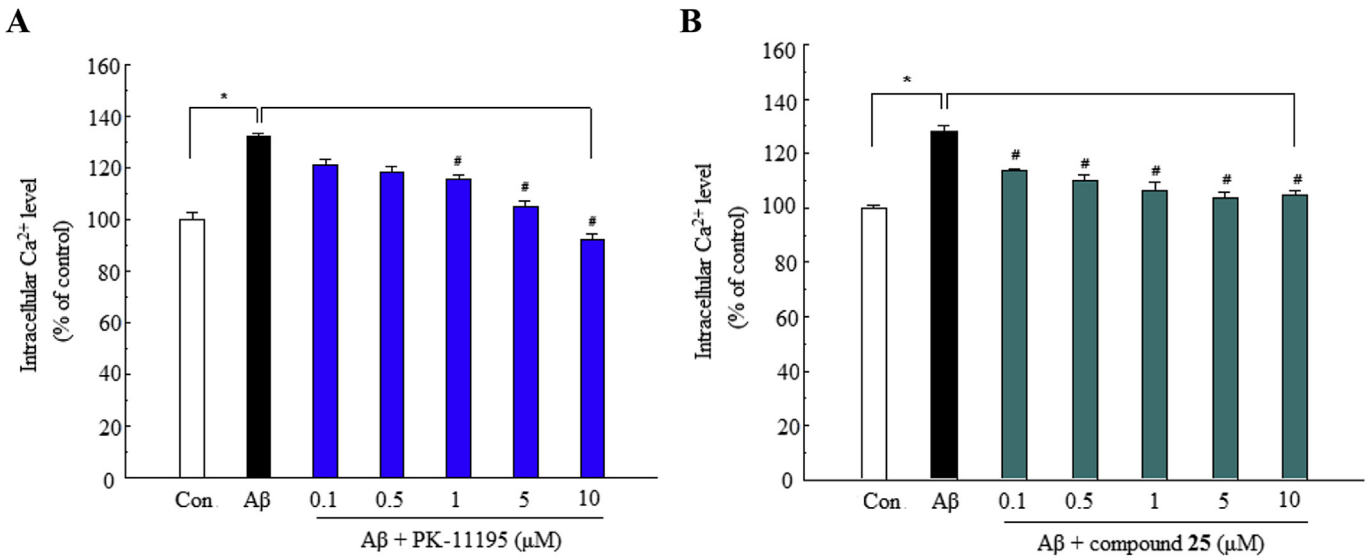

Fig. 2. Alleviation of Aβ-induced increase of intracellular Ca^{2+} level by treating PK-11195 (**A**) or compound **25** (**B**). After the treatment of each compound in HT22 cell, intracellular Ca^{2+} level (% of control) was measured by fluorescence of Fura-2 dye. (#) $p < 0.05$.

environments. Since rodents prefer to seek a new arm of the maze rather than revisit the previously explored one, the number of arm entries and their sequences are recorded to calculate the percent alternation. Therefore, Y-maze tests can quantify cognitive function, and higher percent alternation indicates better spatial learning and memory in acute AD model mice, reversing 72% of the cognitive deficit induced by Aβ, whereas a known nootropic agent, piracetam only restored 20% (Fig. 3A). Compound **38** also reversed 62% of the Aβ induced memory deficit, whereas piracetam reversed 32% (Fig. 3B). Overall, both compounds **25** and **38** successfully

improved spatial working memory function by ameliorating the cognitive deficit induced by Aβ in mice.

2.9. Contextual fear conditioning test in transgenic AD model mice

As observed in the Y-maze spontaneous alternation test, the treatment of compound **25** alleviated learning and memory deficits in acute AD mice to an extent similar to wild type mice. To further assess neuroprotective effects of compound **25**, we decided to perform contextual fear conditioning tests by using a transgenic mouse model of AD, APPswe/PSEN1dE9 2X (11 months, n = 7). For testing, we orally administered compound **25** for 1 month (30 mg/kg daily), and then carried out contextual fear conditioning tests by following the previously reported procedures [34]. We measured the number of total freezing responses of the mice in response to fear-relevant stimuli, and higher freezing percent indicates better cognitive function. As demonstrated in Fig. 4, compound **25** partially restored fear-associated learning and memory, reversing 12% of cognitive deficits in transgenic mice, whereas piracetam did not affect behavior of the tested mice. Based on these results, we believe that compound **25** is capable of reversing learning and memory deficits in acute and transgenic mice models of AD.

2.10. Pharmacokinetics of compound 25

To further validate in vivo activity of compound **25**, we evaluated its pharmacokinetic profile in Sprague-Dawley (SD) male rats (Table 6). Compound **25** demonstrated relatively high brain-to-plasma (B/P) ratio (2.88) after 2 h of its intravenous injection, indicating that compound **25** is blood brain barrier (BBB) permeable. However, compound **25** exhibited unexpectedly low oral bioavailability (3.7%) and low plasma concentration when administered orally. This low oral bioavailability may explain the relatively lower percent efficacy of **25** in orally administrated Tg mice (12%, Fig. 4) compared to the efficacy in intraperitoneally injected acute AD model mice (72%, Fig. 3A). Therefore, our future efforts for further optimization will be focused on the improvement of the pharmacokinetic profiles, particularly oral bioavailability.

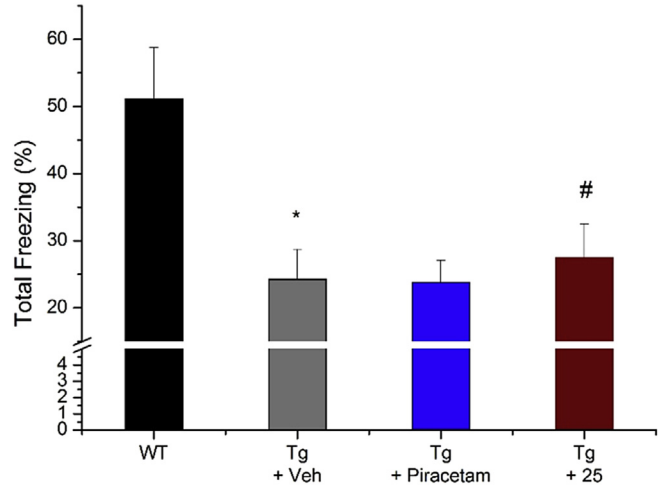

Fig. 4. Alleviation of emotion-associated learning memory in Tg AD model mice by treating compounds **25**. The therapeutic effect of compound **25** (30 mg/kg daily, 1 month) on emotional learning and memory in APPswe/PSEN1dE9 2x transgenic model (12 month, n = 7) was assessed by contextual fear conditioning test compared to piracetam (30 mg/kg daily, 1 month). Data are mean ± SEM (n = 7 per group): (*) $p < 0.01$, compared with WT, (#) $p < 0.05$, compared with vehicle-treated transgenic AD model mice.

2.11. Interaction of compound 25 with the 18 kDa TSPO

Our in vitro and in vivo tests indicate that compound **25** exerts neuroprotective effects by blocking Aβ-induced mPTP opening, in which the 18 kDa TSPO participates. To verify whether the neuroprotective effects of compound **25** is derived from the binding of TSPO, we measured the binding affinity of **25** for purified TSPO by

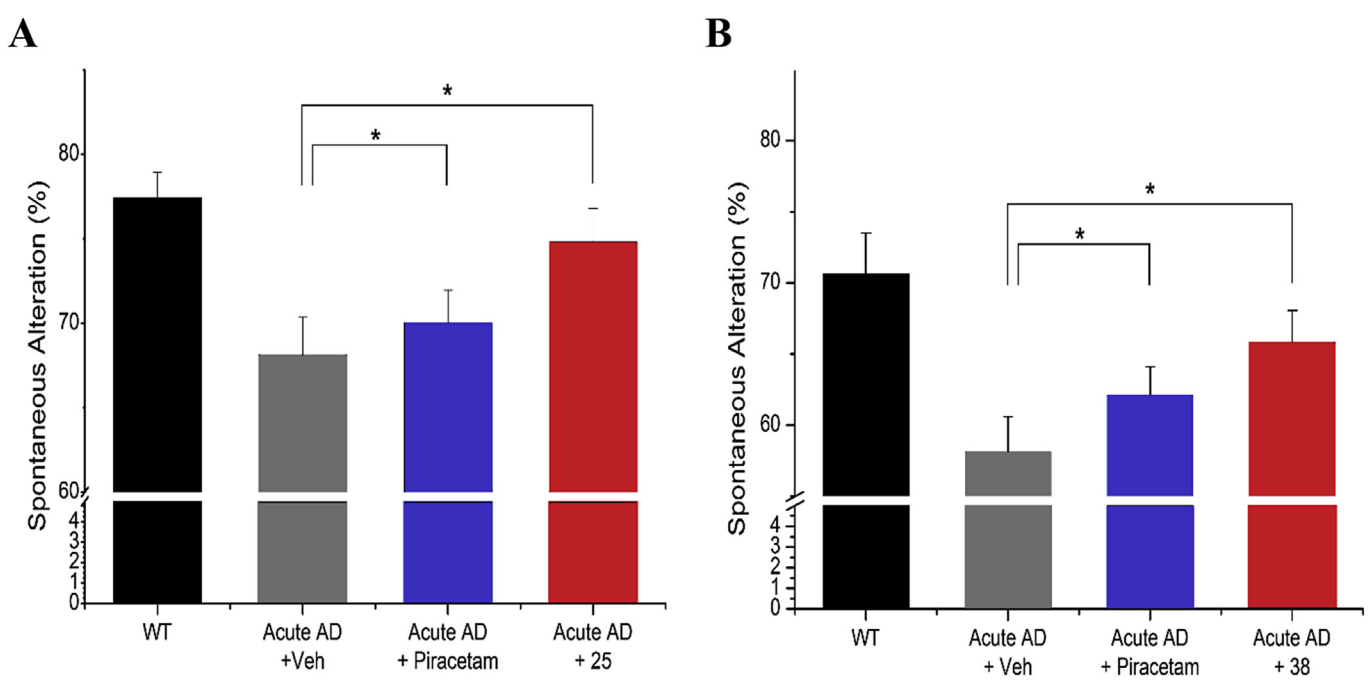

Fig. 3. Alleviation of learning and memory deficits in acute AD model mice by treating compounds **25** or **38**. The effects of compounds **25** (A) or **38** (B) (30 mg/kg daily, 6 days, i.p.) on learning and memory deficits in acute AD model mice was assessed by Y-maze spontaneous alternation test. Each compound was individually evaluated comparing with piracetam (30 mg/kg daily, 6 days, i.p.). Data are mean ± SEM (n = 7 per group): (*) $p < 0.05$.

Table 6
Mean (±SD) pharmacokinetic parameters[a] after intravenous ($n = 4$) and oral ($n = 5$) administration (10 mg/kg) of compound **25** to SD male rats.

Plasma	Intravenous	Oral
$AUC_{0-\infty}$ (μg min/ml)	111.02 ± 45.06	8.17 ± 2.51
AUC_{last} (μg min/ml)	104.75 ± 45.41	7.68 ± 2.53
Terminal half-life (min)	157.48 ± 126.04	89.25 ± 21.68
C_{max} (μg/ml)	–	0.07 ± 0.01
T_{max} (min)	–	33
CL (mL/mim/kg)	54.55 ± 31.38	–
MRT (min)	67.14 ± 28.87	–
V_{ss} (mL/kg)	6205.39 ± 5089.22	–
Ae (%)	0.03	0.01
Brain-to-plasma ratio (B/P) at 2 h	2.88	1.02
F (%)		3.7

[a] $AUC_{0-\infty}$, total area under the plasma concentration–time curve from time zero to time infinity; AUC_{last}, total area under the plasma concentration–time curve from time zero to last measured time; C_{max}, peak plasma concentration; T_{max}, time to reach C_{max}; CL, time-averaged total body clearance; MRT, mean residence time; V_{ss}, apparent volume of distribution at steady state; *Ae*, Excreted amount; *F*, bioavailability.

using [^{3}H] PK-11195 as a competitive ligand. As shown in Table 7, compound **25** appeared to be a potent ligand for TSPO, exhibiting K_i and IC_{50} values in a low nanomolar range ($K_i = 22.8 \pm 10.6$ nM, $IC_{50} = 74.3 \pm 14.7$ nM). Additionally, we performed surface plasmon resonance (SPR) measurements to analyze the interaction of compound **25** with recombinant human TSPO (Fig. 5). The SPR data indicate that compound **25** interacts with the human TSPO demonstrating the K_D value of 108 nM. **PK-11195** showed a lower K_D value (11.1 nM), which corresponds to the results from competitive binding assays. Although the binding affinity of compound **25** is not superior to that of **PK-11195**, these results support our hypothesis that the neuroprotective effects of compound **25** come from its binding to the TSPO.

To investigate the binding mode of compound **25**, we performed molecular docking studies by using a homology model of human TSPO (Fig. 6). Since crystal structure of human TSPO has not been reported yet, the most reliable homology model of human TSPO was generated by using recently reported crystal structure of the bacterial TSPO (PDB ID: 4RYI). It has been suggested that PK-11195 fits in the central cavity of TSPO [35], therefore, we also docked compound **25** in the same binding site. Both of PK-11195 and compound **25** were docked into the hydrophobic central cavity (indicated as grooves in Fig. 6) of the TSPO with additional hydrogen bond interactions. The predicted binding mode showed that the carbonyl oxygen of **PK-11195** (Glide docking score = −10.80) interacts with the indole-NH groups of Trp53 and Trp143 through two hydrogen bond interactions as shown in Fig. 6A. Also, the Cl atom attached to the phenyl ring of **PK-11195** forms a halogen bond with the oxygen atom of the OH group of Tyr57. Furthermore, the isoquinoline group of **PK-11195** interacts with the rings of Trp95 through hydrophobic π-π interactions. Next, compound **25** was docked into the same binding pocket of **PK-11195** as shown in Fig. 6B (Glide docking score = −9.24). The best fitted pose of compound **25** exhibited hydrogen bond interactions. The amide group of compound **25** forms a hydrogen bond with the indole-NH group of Trp53, which was also observed as a hydrogen bond donor for **PK-11195**. The nitrogen atom of the benzimidazole core forms a hydrogen bond with the OH group of Tyr57, which corresponds to the halogen bond interaction between Tyr57 and Cl atom in **PK-11195**. The benzimidazole group of compound **25** is stacked between the two Trp resides (Trp53 and Trp95), interacting through hydrophobic π-π interactions. In addition, the di-Cl substituted benzyl group attached to the benzimidazole of compound **25** interact with Arg24 through hydrophobic interactions. The 2-methyl 5-isopropyl phenyl group exhibits additional hydrophobic interactions with Phe99. As a result of these binding interactions, we believe that compound **25** competes with **PK-11195** in the same binding site of the TSPO.

Table 7
Inhibition of TSPO.

Compds	IC_{50} (nM)[a]	K_i (nM)[a]
25	74.3 ± 14.7	22.8 ± 10.6
PK-11195	1.32 ± 1.10	8.85 ± 1.09

[a] Values are expressed as the mean ± SD from at least three independent experiments.

3. Conclusion

In this study, we have developed novel benzimidazole derivatives as an mPTP blocker to treat mitochondrial dysfunction in AD. We generated a common feature pharmacophore model based on the structures of the previously reported neuroprotective ligands of TSPO, one of the putative components of the mPTP. To identify a lead compound, we screened our in-house library as well as commercially available chemical libraries against our pharmacophore model, discovering compound **1** as a virtual hit. Based on the structure of compound **1**, we designed and synthesized a library of benzimidazole derivatives, and evaluated biological effects of the newly generated compounds. Among the tested compounds, compound **25** effectively alleviated Aβ-induced mitochondrial dysfunction in cells, recovering the mitochondrial membrane potential, ATP production, cellular viability, and suppressing ROS generation and intracellular calcium levels. More importantly, compound **25** successfully recovered AD-associated cognitive deficits in preclinical AD model mice. Pharmacokinetic studies revealed that compound **25** readily crosses the BBB, and bind to the 18 kDa TSPO located in mitochondrial outer membrane, although its oral bioavailability is relatively low. Competitive binding assays and SPR kinetics indicated that compound **25** binds to TSPO with K_D values of 108 nM, supporting that neuroprotective effects of compound **25** comes from the direct interaction with TSPO. Binding mode analysis also supports that compound **25** interacts with TSPO in the similar manner as a known TSPO ligand, **PK-11195**. In conclusion, compound **25** is a promising lead for the development of modulators of mitochondrial function. We believe that further optimization for more potent and orally bioavailable benzimidazole derivatives may provide a possible therapeutic option for the treatment of neurodegenerative diseases such as AD.

4. Experimental section

4.1. Chemistry

4.1.1. General methods

All reagents were obtained from commercial sources and used without further purification. All reactions were performed under a nitrogen atmosphere in oven-dried glassware. Reactions were monitored by analytical thin-layer chromatography (TLC) plates (Merck, catalog no. 1.05715) with spots visualized by UV light ($\lambda = 254$ nm) or using a KMnO4 solution. Solvents were evaporated using a rotary evaporator under a reduced pressure of 50 mBar. The reaction products were purified by flash column chromatography using silica gel 60 (Merck, catalog nos. 1.07734). Melting points were determined using an OptiMelt melting point apparatus (Stanford Research System, Inc.) in open capillary tube without correction. ^{1}H (300 or 400 MHz) and ^{13}C (75 or 100 MHz) NMR spectra were recorded using tetramethylsilane (TMS) as the

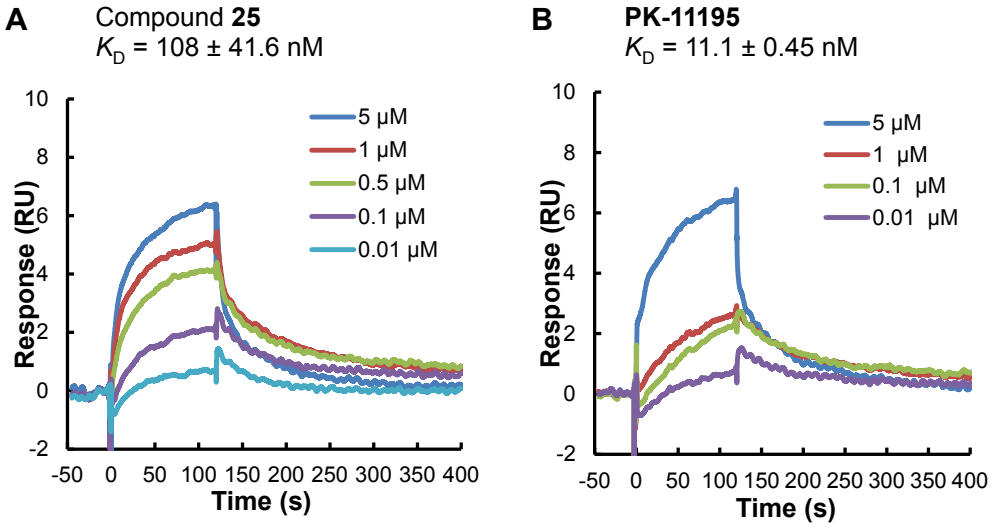

Fig. 5. Representative SPR sensorgrams for compound **25** (**A**) and PK-11195 (**B**). K_D values are expressed as the mean ± SD from at least three independent experiments.

internal standard. Chemical shifts (δ) are reported in parts per million (ppm) values relative to TMS, and the coupling constants (J) are reported in hertz (Hz). The purity (≥95%) of the samples was determined by analytical HPLC using a Waters E2695 system with SunFire C18 column (4.6 mm × 150 mm; 5 μm). HPLC data were recorded using parameters as follows: H_2O/MeCN, 80/20 → 0/100 in 20 min, +3 min isocratic, flow rate of 1.0 mL/min, λ = 254 and 280 nm. High–resolution mass spectra (HRMS) were recorded on a LTQ Orbitrap (Thermo Electron Corporation) instrument. Liquid chromatograph mass spectra (LC/MS) data were recorded on a Shimadzu LCMS-2020 instrument equipped with Shimadzu's VP-ODS column (4.6 mm × 150 mm; 4.6 μm). LC/MS data were recorded using parameters as follows: H_2O/MeCN, 90/10 → 0/100 in 15 min, +3 min isocratic, flow rate of 1.0 mL/min, λ = 254 and 280 nm. Reaction yields are for purified products.

*4.1.2. General procedure for the synthesis of compounds **10**–**32***

To a stirred solution of compound **9** (1.0 equiv) and 1-[bis(dimethylamino)methylene]-1*H*-1,2,3-triazolo[4,5-*b*]pyridinium 3-oxid hexafluorophosphate (HATU, 1.2 equiv) in MeCN was added triethylamine (Et_3N, 5.0 equiv). After 1 h of stirring at room temperature, the desired substituted amine (1.2 equiv) was added dropwise. The reaction mixture was stirred at room temperature for 12–16 h, concentrated in vacuo, and extracted with EtOAc (3 × 30 mL). The organic layer was dried over anhydrous $MgSO_4$, filtered, concentrated, and purified by column chromatography on SiO_2 (*n*-hexane/EtOAc: 1/1). The resultant product was recrystallized with diethyl ether to yield the desired compound.

*4.1.2.1. N-(3,5-Di-tert-butylphenyl)-2-(2-phenyl-1H-benzo[d]imidazol-1-yl)acetamide (**10**).* Following the general procedure for compounds **10**–**32**, 2-(2-phenyl-1*H*-benzo[*d*]imidazol-1-yl)acetic acid **9a** (20 mg, 0.08 mmol), 3,5-di-*tert*-butylaniline (21 mg, 0.10 mmol), HATU (38 mg, 0.10 mmol) and Et_3N (56 μL, 0.40 mmol) in MeCN (3 mL) gave the title compound **10** (21 mg, 60%) as a white solid; R_f = 0.20 (*n*-hexane/EtOAc: 1/1); mp: 238.4–241.5 °C; HPLC purity: 10.58 min, 97.3%; ^{1}H NMR (300 MHz, MeOD) δ 7.78 (m, 2H), 7.71–7.74 (m, 1H), 7.57 (m, 3H), 7.51 (d, J = 5.1 Hz, 1H), 7.45 (m, 2H), 7.32–7.34 (m, 2H), 7.24 (s, 1H), 5.07 (s, 2H), 1.30 (s, 18H); ^{13}C NMR (75 MHz, MeOD) δ 165.86, 154.38, 151.41 (2C), 141.75, 137.27, 136.02, 130.12, 129.34 (2C), 129.20 (2C), 128.63 (2C), 123.22, 122.75, 118.41, 114.31 (2C), 110.09, 47.03 (overlapped with MeOD peaks), 34.39 (2C), 30.42 (6C); HRMS (ESI$^+$): *m/z*: calcd for $C_{29}H_{34}N_3O$ 440.2624 [M+H]$^+$; found: 440.2696.

*4.1.2.2. N-(5-Isopropyl-2-methylphenyl)-2-(2-phenyl-1H-benzo[d]imidazol-1-yl)acetamide (**11**).* Following the general procedure for compounds **10**–**32**, 2-(2-phenyl-1*H*-benzo[*d*]imidazol-1-yl)acetic acid **9a** (20 mg, 0.08 mmol), 5-iso-propyl-2-methylaniline (15 mg, 0.10 mmol), HATU (38 mg, 0.10 mmol), and Et_3N (56 μL, 0.40 mmol) in MeCN (3 mL) gave the title compound **11** (11 mg, 35%) as a white solid; R_f = 0.20 (*n*-hexane/EtOAc: 1/1); mp: 129.0–132.9 °C; HPLC purity: 16.84 min, 99.9%; ^{1}H NMR (400 MHz, MeOD) δ 7.82–7.83 (m, 2H), 7.75 (d, J = 7.6 Hz, 1H), 7.61–7.63 (m, 4H), 7.35–7.43 (m, 2H), 7.15–7.17 (m, 2H), 7.05 (d, J = 7.2 Hz, 1H), 5.19 (s, 2H), 2.85 (septet, J = 7.2 Hz, 1H), 2.18 (s, 3H), 1.23 (d, J = 6.8 Hz, 6H); ^{13}C NMR (101 MHz, MeOD) δ 166.69, 147.13, 141.87, 136.08, 134.59, 130.20, 130.15 (2C), 129.47, 129.24 (2C), 128.64 (2C), 124.45, 123.41, 123.21, 122.76, 118.48, 113.23, 110.07, 47.17 (overlapped with MeOD peaks), 33.48, 22.95 (2C), 16.33; HRMS (ESI$^+$): *m/z*: calcd for $C_{25}H_{26}N_3O$ 384.1998 [M+H]$^+$; found: 384.2069.

*4.1.2.3. N-(3,5-Dichlorophenyl)-2-(2-phenyl-1H-benzo[d]imidazol-1-yl)acetamide (**12**).* Following the general procedure for compounds **10**–**32**, 2-(2-phenyl-1*H*-benzo[*d*]imidazol-1-yl)acetic acid **9a** (30 mg, 0.12 mmol), 3,5-dichloroaniline (25 mg, 0.15 mmol), HATU (91 mg, 0.24 mmol), and Et_3N (86 μL, 0.60 mmol) in MeCN (3 mL) gave the title compound **12** (24 mg, 50%) as a white solid; R_f = 0.30 (*n*-hexane/EtOAc: 1/1); mp: 236.6–238.8 °C; HPLC purity: 19.44 min, 99.8%; ^{1}H NMR (300 MHz, MeOD) δ 7.75 (m, 3H), 7.60 (m, 5H), 7.51–7.53 (m, 1H), 7.36–7.38 (m, 2H), 7.19 (s, 1H), 5.11 (s, 2H); ^{13}C NMR (101 MHz, DMSO-d_6) δ 166.93, 154.01, 142.92, 141.17, 136.91, 134.69 (2C), 130.45, 120.32, 129.58 (2C), 129.29 (2C), 123.53, 123.18, 122.70, 119.63, 118.00 (2C), 111.09, 48.20; HRMS (ESI$^+$): *m/z*: calcd for $C_{21}H_{16}Cl_2N_3O$ 396.0592 [M+H]$^+$; found: 396.0663.

*4.1.2.4. N-(2-tert-Butyl-6-methylphenyl)-2-(2-phenyl-1H-benzo[d]imidazol-1-yl)acetamide (**13**).* Following the general procedure for compounds **10**–**32**, 2-(2-phenyl-1*H*-benzo[*d*]imidazol-1-yl)acetic acid **9a** (30 mg, 0.12 mmol), 2-*tert*-butyl-6-methylaniline (78 mg, 0.48 mmol), HATU (91 mg, 0.24 mmol), and Et_3N (84 μL, 0.48 mmol) in MeCN (3 mL) gave the title compound **13** (36 mg, 78%) as a white solid; R_f = 0.25 (*n*-hexane/EtOAc: 1/1); mp: 213.6–215.9 °C; HPLC purity: 15.39 min, 99.1%; ^{1}H NMR (400 MHz, $CDCl_3$) δ 7.90 (m, 3H),

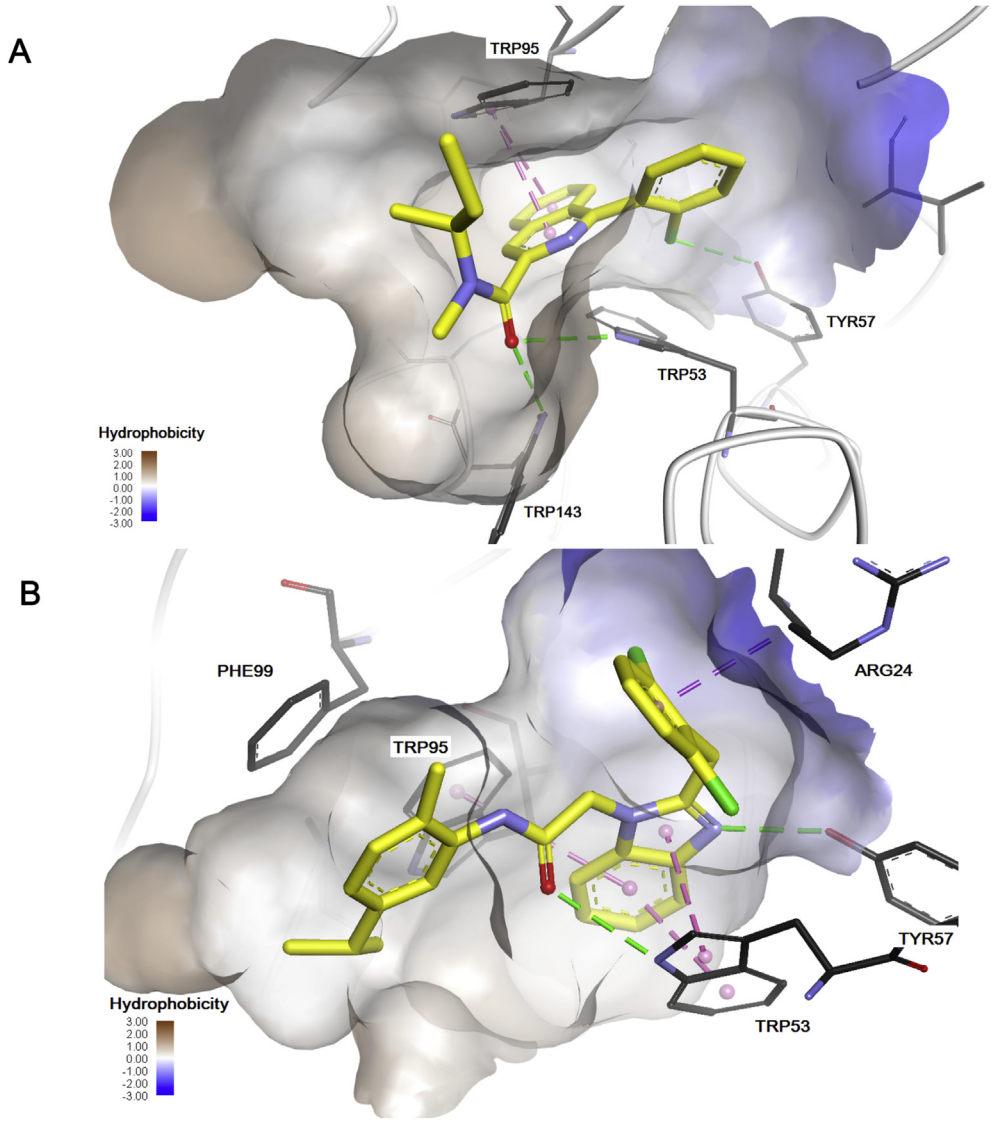

Fig. 6. Binding modes of PK-11195 (**A**) and compound **25** (**B**) with the homology model of human TSPO built on a crystal structure of the bacterial TSPO (PDB ID: 4RYI). The predicted binding mode demonstrated that PK-11195 and compound **25** form several hydrogen bond interactions (indicated in green lines) and hydrophobic interactions (indicated in pink lines). (Carbon atoms in yellow, Oxygen atom in red, Nitrogen atom in blue, and Chlorine atom in green). (For interpretation of the references to colour in this figure legend, the reader is referred to the web version of this article.)

7.54–7.60 (m, 4H), 7.44–7.50 (m, 2H), 7.21 (d, J = 7.6 Hz, 1H), 7.08–7.12 (m, 2H), 6.73 (br s, 1H), 5.22 (s, 2H), 2.05 (s, 3H), 1.10 (s, 9H); ^{13}C NMR (75 MHz, $CDCl_3$) δ 165.57, 153.67, 146.61, 143.32, 137.61, 135.49, 132.32, 130.52, 129.56 (2C), 129.21 (2C), 129.13 (2C), 128.11, 124.79, 123.86, 123.71, 120.62, 110.07, 48.54, 34.90, 30.63 (3C), 18.95; HRMS (ESI$^+$): m/z: calcd for $C_{26}H_{28}N_3O$ 398.2227 [M+H]$^+$; found: 398.2218.

*4.1.2.5. N-(5-Isopropyl-2-methylphenyl)-2-(2-phenyl-1H-benzo[d]imidazol-1-yl)acetamide (**14**).* Following the general procedure for compounds **10**–**32**, 2-(2-(2,5-dichlorophenyl)-1*H*-benzo[*d*]imidazol-1-yl)acetic acid **9b** (50 mg, 0.17 mmol), 5-iso-propyl-2-methylaniline (35 μL, 0.22 mmol), HATU (84 mg, 0.22 mmol), and Et_3N (119 μL, 0.85 mmol) in MeCN (7 mL) gave the title compound **14** (23 mg, 33%) as a white solid; R_f = 0.25 (*n*-hexane/EtOAc: 2/1); mp: 185.1–188.2 °C; HPLC purity: 19.38 min, 99.7%; ^{1}H NMR (300 MHz, MeOD) δ 7.74–7.75 (m, 1H), 7.64–7.69 (m, 4H), 7.38–7.44 (m, 2H), 7.08–7.10 (m, 2H), 7.03 (m, 1H), 5.08 (s, 2H), 2.83 (septet, J = 6.9 Hz, 1H), 2.10 (s, 3H), 1.20 (d, J = 7.2 Hz, 6H); ^{13}C NMR (75 MHz, MeOD) δ 166.00, 150.13, 147.09, 141.79, 135.32, 134.45, 132.90, 132.48, 132.26, 131.90, 131.10, 130.58, 130.16, 130.10, 124.44, 123.90, 123.40, 122.89, 118.84, 110.28, 46.22, 33.45, 22.93 (2C), 16.25; HRMS (ESI$^+$): m/z: calcd for $C_{25}H_{24}Cl_2N_3O$ 452.1218 [M+H]$^+$; found: 452.1288.

*4.1.2.6. N-(3,5-Dichlorophenyl)-2-(2-(2,5-dichlorophenyl)-1H-benzo[d]imidazol-1-yl)acetamide (**15**).* Following the general procedure for compounds **10**–**32**, 2-(2-(2,5-dichlorophenyl)-1*H*-benzo[*d*]imidazol-1-yl)acetic acid **9b** (45 mg, 0.14 mmol), 3,5-dichloroaniline (29 mg, 0.18 mmol), HATU (160 mg, 0.42 mmol), and Et_3N (98 μL, 0.70 mmol) in MeCN (5 mL) gave the title compound **15** (30 mg, 40%) as a white solid; R_f = 0.25 (*n*-hexane/EtOAc: 2/1); mp: 215.0–219.1 °C; 19.37 min, 99.2%; ^{1}H NMR (300 MHz, MeOD) δ 7.60 (m, 1H), 7.67–7.68 (m, 1H), 7.62–7.64 (m, 3H), 7.58 (m, 2H), 7.41–7.51 (m, 2H), 7.16–7.18 (m, 1H), 5.01 (s, 2H); ^{13}C NMR (75 MHz, MeOD) δ 165.62, 150.10, 141.73, 140.00, 135.24, 134.90

(2C), 132.93, 132.44, 132.22, 131.91, 131.04, 130.42, 123.76, 123.60, 122.93, 118.83 (2C), 117.70, 110.26, 46.73 (overlapped with MeOD peaks); HRMS (ESI$^+$): *m/z*: calcd for $C_{21}H_{14}Cl_4N_3O$ 463.9885 [M+H]$^+$; found: 463.9872.

*4.1.2.7. N-(2-tert-Butyl-6-methylphenyl)-2-(2-(2,5-dichlorophenyl)-1H-benzo[d]imidazol-1-yl)acetamide (**16**).* Following the general procedure for compounds **10**–**32**, 2-(2-(2,5-dichlorophenyl)-1*H*-benzo[*d*]imidazol-1-yl)acetic acid **9b** (26 mg, 0.08 mmol), 2-methyl-6-*tert*-butylaniline (16 mg, 0.10 mmol), HATU (38 mg, 0.10 mmol), and Et_3N (56 μL, 0.40 mmol) in MeCN (3 mL) gave the title compound **16** (21 mg, 57%) as a white solid; R_f = 0.25 (*n*-hexane/EtOAc: 2/1); mp: 193.2–194.6 °C; HPLC purity: 17.74 min, 99.6%; ^{1}H NMR (300 MHz, $CDCl_3$) δ 7.92 (d, *J* = 3.9 Hz, 1H), 7.71 (s, 1H), 7.51–7.57 (m, 3H), 7.44–7.48 (m, 2H), 7.11–7.19 (m, 3H), 6.67 (s, 1H), 5.00 (s, 2H), 2.02 (s, 3H), 1.08 (s, 9H); ^{13}C NMR (75 MHz, Acetone-d_6) δ 165.48, 150.16, 147.59, 143.29, 138.18, 135.83, 134.08, 132.83, 132.51, 132.30, 131.93, 131.50, 131.16, 128.39, 127.44, 124.44, 123.02, 122.24, 119.90, 110.26, 46.49, 34.79, 30.56 (3C), 17.98; HRMS (ESI$^+$): *m/z*: calcd for $C_{26}H_{26}Cl_2N_3O$ 466.1375 [M+H]$^+$; found: 466.1380.

*4.1.2.8. N-(5-(Biphenyl-4-yloxy)-2-fluorophenyl)-2-(2-(2,5-dimethoxyphenyl)-1H-benzo[d]imidazol-1-yl)acetamide (**17**).* Following the general procedure for compounds **10**–**32**, 2-(2-(2,5-dimethoxyphenyl)-1*H*-benzo[*d*]imidazol-1-yl)acetic acid **9c** (72 mg, 0.23 mmol), 5-(biphenyl-4-yloxy)-2-fluoroaniline (82 mg, 0.29 mmol), HATU (110 mg, 0.29 mmol), and Et_3N (130 μL, 0.92 mmol) in MeCN (3 mL) gave the title compound **17** (56 mg, 44%) as a white solid; R_f = 0.20 (*n*-hexane/EtOAc: 2/1); mp: 116.5–119.2 °C; HPLC purity: 12.29 min, 99.4%; ^{1}H NMR (400 MHz, $CDCl_3$) δ 8.41 (dd, *J* = 10.4 Hz, 2.8 Hz, 1H), 8.16 (br s, 1H), 7.73 (d, *J* = 7.6 Hz, 1H), 7.51 (d, *J* = 7.2 Hz, 2H), 7.46 (t, *J* = 7.6 Hz, 2H), 7.37–7.38 (m, 1H), 7.29–7.32 (m, 2H with $CDCl_3$ peak), 7.23 (d, *J* = 6.4 Hz, 1H), 7.19–7.22 (m, 2H), 7.05–7.12 (m, 2H), 6.93–6.96 (m, 2H), 6.82 (td, *J* = 8.0 Hz, 3.2 Hz, 1H), 6.47 (d, *J* = 8.4 Hz, 2H), 4.76 (s, 2H), 3.81 (s, 3H), 3.64 (s, 3H); ^{13}C NMR (101 MHz, $CDCl_3$) δ 165.82, 159.28 (d, ^1J = 241.4 Hz), 156.04, 154.03, 151.99, 151.07, 143.19, 140.27, 140.04, 136.24, 134.85, 130.92 (d, ^3J = 12.1 Hz), 128.77 (2C), 128.35 (2C), 127.09, 126.85 (2C), 123.70, 123.10, 121.02 (d, ^3J = 10.1 Hz), 120.26, 118.59, 118.35, 117.15, 116.27 (2C), 112.31, 110.87 (d, ^2J = 24.2 Hz), 109.30, 107.92 (d, ^2J = 29.3 Hz), 55.92, 55.88, 46.50; HRMS (ESI$^+$): *m/z*: calcd for $C_{35}H_{29}FN_3O_4$ 574.2064 [M+H]$^+$; found: 574.2134.

*4.1.2.9. 2-(2-(2,5-Dimethoxyphenyl)-1H-benzo[d]imidazol-1-yl)eN-(5-isopropyl-2-methylphenyl)acetamide (**18**).* Following the general procedure for compounds **10**–**32**, 2-(2-(2,5-dimethoxyphenyl)-1*H*-benzo[*d*]imidazol-1-yl)acetic acid **9c** (50 mg, 0.13 mmol), 5-isopropyl-2-methylaniline (30 μL, 0.19 mmol), HATU (65 mg, 0.17 mmol), and Et_3N (73 μL, 0.52 mmol) in MeCN (3 mL) gave the title compound **18** (24 mg, 44%) as a white solid; R_f = 0.25 (*n*-hexane/EtOAc: 2/1); mp: 205.4–209.1 °C; HPLC purity: 9.90 min, 99.6%; ^{1}H NMR (400 MHz, MeOD) δ 7.74 (d, *J* = 7.6 Hz, 1H), 7.61 (d, *J* = 7.6 Hz, 1H), 7.35–7.40 (m, 2H), 7.11–7.19 (m, 5H), 7.01 (dd, *J* = 7.6 Hz, 1.6 Hz, 1H), 5.07 (s, 2H), 3.83 (s, 3H), 3.81 (s, 3H), 2.85 (septet, *J* = 6.8 Hz, 1H), 2.07 (s, 3H), 1.22 (d, *J* = 6.8 Hz, 6H); ^{13}C NMR (75 MHz, MeOD) δ 166.55, 153.93, 152.14, 151.52, 147.05, 142.03, 135.72, 134.68, 130.10, 129.66, 124.14, 123.02, 122.98, 122.37, 118.94, 118.35, 117.43, 117.13, 112.68, 110.11, 55.40, 54.90, 47.30 (overlapped with MeOD peaks), 33.46, 22.91 (2C), 16.12; HRMS (ESI$^+$): *m/z*: calcd for $C_{27}H_{30}N_3O_3$ 444.2209 [M+H]$^+$; found: 444.2280.

*4.1.2.10. 2-(2-Benzyl-1H-benzo[d]imidazol-1-yl)eN-(3,5-di-tert-butylphenyl)acetamide (**19**).* Following the general procedure for compounds **10**–**32**, 2-(2-benzyl-1*H*-benzo[*d*]imidazol-1-yl)acetic acid **9d** (30 mg, 0.11 mmol), 3,5-di-*tert*-butylaniline (30 mg, 0.15 mmol), HATU (57 mg, 0.15 mmol), and Et_3N (98 μL, 0.70 mmol) in MeCN (3 mL) gave the title compound **19** (37 mg, 72%) as a white solid; R_f = 0.30 (*n*-hexane/EtOAc: 1/1); mp: 238.9–240.8 °C; HPLC purity: 17.03 min, 100%; ^{1}H NMR (300 MHz, $CDCl_3$) δ 7.84–7.86 (m, 1H), 7.25–7.36 (m, 7H), 7.17–7.20 (m, 2H), 7.05 (s, 2H), 7.00 (s, 1H), 4.80 (s, 2H), 4.32 (s, 2H), 1.27 (s, 18H); ^{13}C NMR (75 MHz, $CDCl_3$) δ 164.28, 153.49, 151.60 (2C), 142.63, 135.76, 135.48, 135.38, 129.23 (2C), 128.48 (2C), 127.50, 123.58, 123.12, 119.91, 119.35, 115.09 (2C), 109.34, 48.02, 34.92 (2C), 34.49, 31.34 (6C); HRMS (ESI$^+$): *m/z*: calcd for $C_{30}H_{36}N_3O$ 454.2780 [M+H]$^+$; found: 454.2853.

*4.1.2.11. 2-(2-Benzyl-1H-benzo[d]imidazol-1-yl)eN-(5-isopropyl-2-methylphenyl)acetamide (**20**).* Following the general procedure for compounds **10**–**32**, 2-(2-benzyl-1*H*-benzo[*d*]imidazol-1-yl)acetic acid **9d** (25 mg, 0.09 mmol), 5-iso-propyl-2-methylaniline (21 mg, 0.12 mmol), HATU (46 mg, 0.12 mmol), and Et_3N (63 μL, 0.45 mmol) in MeCN (3 mL) gave the title compound **20** (27 mg, 73%) as a white solid; R_f = 0.30 (*n*-hexane/EtOAc: 1/1); mp: 213.1–214.3 °C; HPLC purity: 12.50 min, 95.7%; ^{1}H NMR (300 MHz, $CDCl_3$) δ 7.85 (d, *J* = 5.4 Hz, 1H), 7.17–7.36 (m, 10H), 6.89–6.96 (m, 2H), 6.56 (br s, 1H), 4.86 (s, 2H), 4.38 (s, 2H), 2.83 (septet, *J* = 7.2 Hz, 1H), 1.57 (s, 3H), 1.21 (d, *J* = 6.9 Hz, 6H); ^{13}C NMR (75 MHz, $CDCl_3$) δ 164.11, 153.36, 147.68, 142.70, 135.25, 134.89, 133.95, 130.29, 129.19 (2C), 128.49 (2C), 127.48, 126.29, 123.83, 123.65, 123.31, 120.82, 120.21, 109.16, 47.82, 34.55, 33.76, 23.96 (2C), 16.53; HRMS (ESI$^+$): *m/z*: calcd for $C_{26}H_{28}N_3O$ 398.2154 [M+H]$^+$; found: 398.2128.

*4.1.2.12. 2-(2-Benzyl-1H-benzo[d]imidazol-1-yl)eN-(5-(biphenyl-4-yloxy)-2-fluorophenyl)acetamide (**21**).* Following the general procedure for compounds **10**–**32**, 2-(2-benzyl-1*H*-benzo[*d*]imidazol-1-yl)acetic acid **9d** (30 mg, 0.11 mmol), 2-methyl-6-*tert*-butylaniline (42 mg, 0.15 mmol), HATU (57 mg, 0.15 mmol), and Et_3N (77 μL, 0.55 mmol) in MeCN (3 mL) gave the title compound **21** (26 mg, 44%) as a white solid; R_f = 0.50 (*n*-hexane/EtOAc: 1/1); mp: 205.5–207.4 °C; HPLC purity: 17.31 min, 94.9%; ^{1}H NMR (300 MHz, $CDCl_3$) δ 8.05 (d, *J* = 5.1 Hz, 1H), 7.75 (d, *J* = 3.9 Hz, 1H), 7.56 (d, *J* = 3.6 Hz, 2H), 7.47 (t, *J* = 9.0 Hz, 2H), 7.37–7.39 (m, 3H), 7.36 (s, 1H), 7.17–7.20 (m, 5H), 7.09–7.10 (m, 3H), 6.83–6.85 (m, 2H), 6.47 (d, *J* = 4.5 Hz, 2H), 4.76 (s, 2H), 4.26 (s, 2H); ^{13}C NMR (101 MHz, $CDCl_3$) δ 164.31, 158.99 (d, ^1J = 242.5 Hz), 155.79, 153.09, 142.57, 140.24, 140.02, 136.43, 134.94 (d, ^2J = 24.1 Hz), 130.11 (d, ^3J = 12.0 Hz), 129.08 (2C), 128.87 (2C), 128.45 (2C), 128.43 (2C), 127.26, 127.21, 126.86 (2C), 123.56, 123.07, 120.25 (d, ^3J = 9.0 Hz), 120.09, 116.44 (2C), 111.14(d, ^2J = 24.1 Hz), 108.57, 108.34, 108.05, 47.80, 34.60; HRMS (ESI$^+$): *m/z*: calcd for $C_{34}H_{27}FN_3O_2$ 528.2009 [M+H]$^+$; found: 528.2078.

*4.1.2.13. 2-(2-Benzyl-1H-benzo[d]imidazol-1-yl)eN-(2-tert-butyl-6-methylphenyl)acetamide (**22**).* Following the general procedure for compounds **10**–**32**, 2-(2-benzyl-1*H*-benzo[*d*]imidazol-1-yl)acetic acid **9d** (20 mg, 0.075 mmol), 2-methyl-6-*tert*-butylaniline (49 mg, 0.30 mmol), HATU (114 mg, 0.30 mmol), and Et_3N (21 μL, 0.15 mmol) in MeCN (2 mL) gave the title compound **22** (15 mg, 45%) as a white solid; R_f = 0.55 (*n*-hexane/EtOAc: 1/1); mp: 213.2–214.6 °C; HPLC purity: 16.35 min, 99.0%; ^{1}H NMR (300 MHz, $CDCl_3$) δ 7.85 (d, *J* = 5.4 Hz, 1H), 7.27–7.39 (m, 7H with $CDCl_3$ peak), 7.12–7.20 (m, 3H), 6.62 (br s, 1H), 4.87 (s, 2H), 4.46 (s, 2H), 2.17 (s, 3H), 1.14 (s, 9H); ^{13}C NMR (75 MHz, $CDCl_3$) δ 165.39, 152.94, 146.53, 142.84, 137.38, 135.18, 134.90, 132.21, 129.23 (2C), 129.19 (2C), 128.46, 128.16, 127.53, 124.84, 123.53, 123.29, 120.32, 109.37, 47.48, 34.93, 34.58, 30.64 (3C), 19.07; HRMS (ESI$^+$): *m/z*: calcd for $C_{27}H_{30}N_3O$ 412.2311 [M+H]$^+$; found: 412.2313.

*4.1.2.14. N-(3,5-Di-tert-butylphenyl)-2-(2-(3,4-dichlorobenzyl)-1H-benzo[d]imidazol-1-yl)acetamide (**23**).* Following the general procedure for compounds **10**–**32**, 2-(2-(3,4-dichlorobenzyl)-1*H*-benzo[*d*]imidazol-1-yl)acetic acid **9e** (20 mg, 0.06 mmol), 3,5-di-*tert*-butylaniline (18 mg, 0.09 mmol), HATU (46 mg, 0.12 mmol), and Et_3N (25 μL, 0.18 mmol) in MeCN (3 mL) gave the title compound **23** (26 mg, 83%) as a white solid; $R_f = 0.35$ (*n*-hexane/EtOAc: 1/2); mp: 221.4–224.1 °C; HPLC purity: 19.15 min, 96.5%; ^{1}H NMR (300 MHz, $CDCl_3$) δ 7.86–7.90 (m, 1H), 7.43 (s, 1H), 7.32–7.41 (m, 4H), 7.14–7.20 (m, 2H), 7.10 (s, 2H), 6.81 (br s, 1H), 4.83 (s, 2H), 4.32 (s, 2H), 1.29 (s, 18H); ^{13}C NMR (101 MHz, DMSO-d_6) δ 165.44, 153.82, 151.24 (2C), 142.66, 138.49, 138.46, 136.27, 131.48, 131.26, 130.82, 129.95, 129.69, 122.49, 122.05, 119.08, 117.79, 113.91 (2C), 110.55, 46.18, 35.01 (2C), 32.26, 31.65 (6C); HRMS (ESI$^+$): *m*/*z*: calcd for $C_{30}H_{34}Cl_2N_3O$ 522.2001 [M+H]$^+$; found: 522.2069.

*4.1.2.15. 2-(2-(3,4-Dichlorobenzyl)-1H-benzo[d]imidazol-1-yl)eN-(5-isopropyl-2-methylphenyl)acetamide (**24**).* Following the general procedure for compounds **10**–**32**, 2-(2-(3,4-dichlorobenzyl)-1*H*-benzo[*d*]imidazol-1-yl)acetic acid **9e** (20 mg, 0.06 mmol), 5-isopropyl-2-methylaniline (14 mg, 0.09 mmol), HATU (46 mg, 0.12 mmol), and Et_3N (25 μL, 0.18 mmol) in MeCN (3 mL) gave title compound **24** (18 mg, 60%) as a white solid; $R_f = 0.35$ (*n*-hexane/EtOAc: 1/2); mp: 226.3–229.1 °C; HPLC purity: 16.48 min, 95.0%; ^{1}H NMR (300 MHz, MeOD) δ 7.66 (s, 1H), 7.44–7.52 (m, 3H), 7.25–7.31 (m, 3H), 7.13 (m, 2H), 7.02 (s, 1H), 5.15 (s, 2H), 4.39 (s, 2H), 2.87 (septet, $J = 7.2$ Hz, 1H), 2.15 (s, 3H), 1.21 (d, $J = 4.2$ Hz, 6H); ^{13}C NMR (75 MHz, MeOD with 2 drops of DMSO) δ 165.53, 147.04, 141.78, 137.32, 135.87, 134.05, 131.93, 130.97, 130.65 (2C), 130.41 (2C), 129.45, 129.03, 123.99, 123.12, 122.91, 122.48, 118.49, 110.20, 33.56, 32.14, 31.24, 23.43 (2C), 16.83; HRMS (ESI$^+$): *m*/*z*: calcd for $C_{26}H_{26}Cl_2N_3O$ 466.1375 [M+H]$^+$; found: 466.1377.

*4.1.2.16. 2-(2-(2,6-Dichlorobenzyl)-1H-benzo[d]imidazol-1-yl)eN-(5-isopropyl-2-methylphenyl)acetamide (**25**).* Following the general procedure for compounds **10**–**32**, 2-(2-(2,6-dichlorobenzyl)-1*H*-benzo[*d*]imidazol-1-yl)acetic acid **9g** (20 mg, 0.06 mmol), 5-isopropyl-2-methylaniline (21 mg, 0.10 mmol), HATU (46 mg, 0.12 mmol), and Et_3N (17 μL, 0.12 mmol) in MeCN (3 mL) gave the title compound **25** (33 mg, 95%) as a white solid; $R_f = 0.40$ (*n*-hexane/EtOAc: 1/1); mp: 250.5–253.6 °C; HPLC purity: 17.59 min, 95.2%; ^{1}H NMR (300 MHz, DMSO-d_6) δ 9.85 (br s, 1H), 7.48–7.58 (m, 4H), 7.37–7.42 (m, 1H), 7.32 (s, 1H), 7.20–7.25 (m, 1H), 7.12–7.16 (m, 2H), 6.99 (d, $J = 7.8$ Hz, 1H), 5.32 (s, 2H), 4.54 (s, 2H), 2.82 (septet, $J = 7.2$ Hz, 1H), 2.22 (s, 3H), 1.15 (d, $J = 6.9$ Hz, 6H); ^{13}C NMR (75 MHz, DMSO-d_6) δ 165.92, 152.29, 146.77, 142.52, 136.33, 136.01, 135.97 (2C), 133.65, 130.79, 129.91, 129.48, 128.80 (2C), 124.04, 123.15, 122.37, 121.87, 119.06, 110.19, 46.43, 33.43, 30.02, 24.32 (2C), 17.95; HRMS (ESI$^+$): *m*/*z*: calcd for $C_{26}H_{26}Cl_2N_3O$ 466.1375 [M+H]$^+$; found: 466.1361.

*4.1.2.17. N-(3,5-Di-tert-butylphenyl)-2-(2-(2,5-dimethoxybenzyl)-1H-benzo[d]imidazol-1-yl)acetamide (**26**).* Following the general procedure for compounds **10**–**32**, 2-(2-(2,5-dimethoxybenzyl)-1*H*-benzo[*d*]imidazol-1-yl)acetic acid **9f** (20 mg, 0.06 mmol), 3,5-di-*tert*-butylaniline (16 mg, 0.08 mmol), HATU (46 mg, 0.12 mmol), and Et_3N (17 μL, 0.12 mmol) in MeCN (3 mL) gave the title compound **26** (27 mg, 86%) as a white solid; $R_f = 0.60$ (*n*-hexane/EtOAc: 1/1); mp: 194.4–197.2 °C; HPLC purity: 10.39 min, 95.1%; ^{1}H NMR (300 MHz, MeOD) δ 7.61 (m, 1H), 7.36–7.42 (m, 1H), 7.37 (s, 2H), 7.20–7.26 (m, 3H), 6.84 (d, $J = 8.4$ Hz, 1H), 6.71–6.75 (m, 2H), 5.02 (s, 2H), 4.29 (s, 2H), 3.76 (s, 3H), 3.61 (s, 3H), 1.29 (s, 18H); ^{13}C NMR (75 MHz, MeOD) δ 165.29, 154.52, 153.81, 151.29 (2C), 151.06, 141.26, 137.28, 135.70, 124.69, 122.60, 122.15, 118.13, 117.76, 115.89, 114.32 (2C), 112.90, 111.46, 109.54, 55.15, 54.63, 45.95, 34.38 (2C), 30.43 (6C), 27.31; HRMS (ESI$^+$): *m*/*z*: calcd for $C_{32}H_{40}N_3O_3$ 514.2991 [M+H]$^+$; found: 514.3063.

*4.1.2.18. 2-(2-(2,5-Dimethoxybenzyl)-1H-benzo[d]imidazol-1-yl)eN-(5-isopropyl-2-methylphenyl)acetamide (**27**).* Following the general procedure for compounds **10**–**32**, 2-(2-(2,5-dimethoxybenzyl)-1*H*-benzo[*d*]imidazol-1-yl)acetic acid **9f** (20 mg, 0.06 mmol), 5-isopropyl-2-methylaniline (12 mg, 0.08 mmol), HATU (46 mg, 0.12 mmol), and Et_3N (17 μL, 0.12 mmol) in MeCN (3 mL) gave the title compound **27** (20 mg, 72%) as a white solid; $R_f = 0.50$ (*n*-hexane/EtOAc: 1/1); mp: 161.6–163.2 °C; HPLC purity: 16.46 min, 95.8%; ^{1}H NMR (300 MHz, MeOD) δ 7.66 (m, 1H), 7.47 (m, 1H), 7.28–7.31 (m, 2H), 7.16 (s, 1H), 7.11 (d, $J = 7.8$ Hz, 1H), 7.01 (m, 1H), 6.92 (d, $J = 8.1$ Hz, 1H), 6.74–6.80 (m, 2H), 5.13 (s, 2H), 4.32 (s, 2H), 3.81 (s, 3H), 3.64 (s, 3H), 2.83 (septet, $J = 7.2$ Hz, 1H), 2.12 (s, 3H), 1.21 (dd, $J = 6.9$ Hz, 4.5 Hz, 6H); ^{13}C NMR (75 MHz, MeOD) δ 166.00, 154.47, 153.88, 151.01, 147.05, 141.18, 135.43, 134.62, 130.10, 124.69, 124.11, 122.99, 122.73 (2C), 122.35, 117.82, 115.79, 112.85, 111.56, 109.55, 55.17, 54.60, 45.78, 33.52, 27.24, 22.96 (2C), 16.18; HRMS (ESI$^+$): *m*/*z*: calcd for $C_{28}H_{32}N_3O_3$ 458.2438 [M+H]$^+$; found: 458.2436.

*4.1.2.19. N-(3,5-Dichlorophenyl)-2-(2-(2,5-dimethoxybenzyl)-1H-benzo[d]imidazol-1-yl)acetamide (**28**).* Following the general procedure for compounds **10**–**32**, 2-(2-(2,5-dimethoxybenzyl)-1*H*-benzo[*d*]imidazol-1-yl)acetic acid **9f** (20 mg, 0.06 mmol), 3,5-dichloroaniline (15 mg, 0.20 mmol), HATU (46 mg, 0.12 mmol), and Et_3N (17 μL, 0.12 mmol) in MeCN (3 mL) gave the title compound **28** (19 mg, 44%) as a white solid; $R_f = 0.50$ (*n*-hexane/EtOAc: 1/1); mp: 223.9–225.1 °C; HPLC purity: 10.11 min, 96.5%; ^{1}H NMR (300 MHz, $CDCl_3$) δ 7.94 (s, 1H), 7.69–7.70 (m, 1H), 7.27–7.29 (m, 2H), 7.22 (s, 2H), 7.02 (s, 1H), 6.80 (m, 1H), 6.70 (d, $J = 9.0$ Hz, 1H), 6.58–6.61 (m, 1H), 4.92 (s, 2H), 4.24 (s, 2H), 3.76 (s, 3H), 3.60 (s, 3H); ^{13}C NMR (75 MHz, $CDCl_3$) δ 165.05, 154.38, 153.82, 150.35, 138.83, 135.20, 134.84 (2C), 124.60, 124.49, 124.44, 123.56, 123.16, 119.32, 118.26 (2C), 116.58, 112.76, 111.98, 109.31, 56.17, 55.47, 47.59, 27.24; HRMS (ESI$^+$): *m*/*z*: calcd for $C_{24}H_{22}Cl_2N_3O_3$ 470.1032 [M+H]$^+$; found: 470.1029.

*4.1.2.20. 2-(5-Chloro-2-(2,5-dichlorophenyl)-1H-benzo[d]imidazol-1-yl)eN-(5-iso-propyl-2-methyl phenyl)acetamide (**29**) and 2-(6-chloro-2-(2,5-dichlorophenyl)-1H-benzo[d]imidazol-1-yl)eN-(5-iso-propyl-2-methyl phenyl)acetamide (**30**).* Following the general procedure for compounds **10**–**32**, an 1:1 mixture of 2-(5-chloro-2-(2,5-dichlorophenyl)-1*H*-benzo[*d*]imidazol-1-yl)acetic acid and methyl 2-(6-chloro-2-(2,5-dichlorophenyl)-1*H*-benzo[*d*]imidazol-1-yl)acetic acid **9h** (40 mg, 0.11 mmol), 5-iso-propyl-2-methylaniline (35 mg, 0.17 mmol), HATU (84 mg, 0.22 mmol), and Et_3N (46 μL, 0.33 mmol) in MeCN (4 mL) gave the mixture of title compounds **29** and **30** (1:1). Two title compounds were separated by column chromatography on SiO_2 (diethyl ether/CH_2Cl_2: 1/40) and confirmed by 2D NOE spectroscopy. Compound **29**; white solid (20 mg, 45%); mp: 213.2–214.2 °C; HPLC purity: 16.35 min, 95.2%; ^{1}H NMR (300 MHz, MeOD) δ 7.76 (d, $J = 1.8$ Hz, 1H), 7.67 (m, 3H), 7.64 (s, 1H), 7.42 (dd, $J = 8.7$ Hz, 2.1 Hz, 1H), 7.09–7.13 (m, 2H), 7.01 (dd, $J = 7.8$ Hz, 1.8 Hz, 1H), 5.09 (s, 2H), 2.83 (septet, $J = 7.2$ Hz, 1H), 2.03 (s, 3H), 1.20 (d, $J = 6.9$ Hz, 6H); ^{13}C NMR (75 MHz, DMSO-d_6) δ 165.36, 162.34, 151.02, 146.69, 141.54, 137.01, 135.68, 132.55 (2C), 132.40, 132.01, 131.20, 130.69, 129.65, 128.12, 124.13, 123.32, 123.05, 121.26, 111.74, 47.12, 33.38, 24.29 (2C), 17.67; HRMS (ESI$^+$): *m*/*z*: calcd for $C_{25}H_{23}Cl_3N_3O$ 486.0901 [M+H]$^+$; found: 486.0898. Compound **30**; white solid (20 mg, 45%); mp: 211.9–213.3 °C; HPLC purity: 16.67 min, 95.1%; ^{1}H NMR (300 MHz, MeOD) δ 7.82 (br s, 1H), 7.74 (d, $J = 4.5$ Hz, 1H), 7.71 (m, 3H), 7.39 (d, $J = 7.5$ Hz, 1H), 7.12 (d, $J = 7.8$ Hz, 1H), 7.09 (s, 1H), 7.02 (dd, $J = 7.8$ Hz, 1.5 Hz, 1H), 5.09 (s,

2H), 2.83 (septet, $J = 7.2$ Hz, 1H), 2.11 (s, 3H), 1.21 (d, $J = 6.9$ Hz, 6H); ^{13}C NMR (75 MHz, DMSO-d_6) δ 165.31, 151.43, 146.68, 143.58, 135.67, 135.06, 132.41 (2C), 132.03, 131.19, 130.69, 129.64, 127.18, 124.11, 123.71, 123.30, 119.36, 113.05, 47.12, 33.38, 24.29 (2C),17.67; HRMS (ESI$^+$): m/z: calcd for $C_{25}H_{23}Cl_3N_3O$ 486.0901 [M+H]$^+$; found: 486.0898.

*4.1.2.21. 2-(5-Chloro-2-(2,5-dichlorophenyl)-1H-benzo[d]imidazol-1-yl)eN-(3,5-dichlorophenyl)acetamide (**31**) and 2-(6-chloro-2-(2,5-dichlorophenyl)-1H-benzo[d]imidazol-1-yl)eN-(3,5-dichlorophenyl) acetamide (**32**).* Following the general procedure for compounds **10**–**32**, an 1:1 mixture of 2-(5-chloro-2-(2,5-dichlorophenyl)-1*H*-benzo[*d*]imidazol-1-yl)acetic acid and methyl 2-(6-chloro-2-(2,5-dichlorophenyl)-1*H*-benzo[*d*]imidazol-1-yl)acetic acid **9h** (47 mg, 0.13 mmol), 3,5-dichloroaniline (32 mg, 0.20 mmol), HATU (84 mg, 0.22 mmol), and Et_3N (46 μL, 0.33 mmol) in MeCN (4 mL) gave the mixture of title compounds **31** and **32** (1:1). Two title compounds were separated by column chromatography on SiO_2 (diethyl ether/CH_2Cl_2: 1/40) and confirmed by 2D NOE spectroscopy. Compound **31**; white solid (20 mg, 66%); mp: 289.9–291.7 °C; HPLC purity: 17.24 min, 98.7%; ^{1}H NMR (400 MHz, DMSO-d_6) δ 10.60 (br s, 1H), 7.87 (s, 1H), 7.69–7.78 (m, 3H), 7.66 (s, 1H), 7.53 (s, 2H), 7.32–7.36 (m, 2H), 5.04 (s, 2H); ^{13}C NMR (101 MHz, DMSO-d_6) δ 165.98, 150.85, 141.55, 140.66, 136.89, 134.68 (2C), 132.48 (2C), 132.41, 132.04, 130.94, 128.48, 123.58, 123.23, 121.30 (2C), 117.90, 111.82, 110.12, 47.61; HRMS (ESI$^+$): m/z: calcd for $C_{21}H_{13}Cl_5N_3O$ 497.9496 [M+H]$^+$; found: 497.9498. Compound **32**; white solid (20 mg, 66%); mp: 288.6–290.6 °C; HPLC purity: 17.30 min, 95.5%; ^{1}H NMR (300 MHz, $CDCl_3$) δ 7.74 (m, 2H), 7.65 (m, 3H), 7.51 (d, $J = 1.8$ Hz, 2H), 7.40 (d, $J = 10.5$ Hz, 1H), 7.19 (m, 1H), 5.01 (s, 2H); ^{13}C NMR (101 MHz, DMSO-d_6) δ 165.99, 151.40, 143.59, 140.93, 134.89, 134.68 (2C), 132.48 (2C), 132.40, 132.05, 128.23, 127.32, 123.86, 123.56, 119.40, 117.91 (2C), 113.16, 111.90, 47.69; HRMS (ESI$^+$): m/z: calcd for $C_{21}H_{13}Cl_5N_3O$ 497.9496 [M+H]$^+$; found: 497.9491.

*4.1.3. General procedure for the synthesis of compound **36**–**44***

To a stirred solution of 4-((2-(2,6-dichlorobenzyl)-1*H*-benzo[*d*]imidazol-1-yl)methyl)benzoic acid **35** (1.0 equiv) in CH_2Cl_2 was added oxalyl chloride (2.0 equiv) dropwise at room temperature. After catalytic amount of DMF (0.2 equiv) was added, the reaction mixture was stirred for 2 h at room temperature. And then, the reaction mixture was concentrated in vacuo. To the resulting residue was added a mixture of the desired substituted amine (1.2 equiv) and DIPEA (2.5 equiv) in THF. The reaction mixture was stirred at room temperature for 16 h, concentrated in vacuo, and extracted with CH_2Cl_2 (3 × 30 mL). The organic layer was dried over anhydrous Na_2SO_4, filtered, concentrated, and purified by column chromatography on SiO_2 (CH_2Cl_2/MeOH: 10/1).

*4.1.3.1. 4-((2-(2,6-Dichlorobenzyl)-1H-benzo[d]imidazol-1-yl) methyl)eN-((1-ethylpyrrolidin-2-yl)methyl)benzamide (**36**).* Following the general procedure for compounds **36**–**44**, 4-((2-(2,6-dichlorobenzyl)-1H-benzo[*d*]imidazol-1-yl)methyl)benzoic acid **35** (100 mg, 0.24 mmol), oxalyl chloride (42 μL, 0.48 mmol), (1-ethylpyrrolidin-2-yl)methanamine (31 μL, 0.26 mmol), and DIPEA (86 μL, 0.60 mmol) gave the title product **36** as a white solid (100 mg, 79%); $R_f = 0.40$ (CH_2Cl_2/MeOH: 10/1); mp: 160.1–162.8 °C; HPLC purity: 7.87 min, 98.7%; ^{1}H NMR (300 MHz, $CDCl_3$) δ 7.76 (dd, $J = 8.1$ Hz, 4.5 Hz, 3H), 7.30–7.31 (m, 2H), 7.23–7.25 (m, 3H), 7.11–7.17 (m, 3H), 7.04 (br s, 1H), 5.50 (s, 2H), 4.48 (s, 2H), 3.65–3.69 (m, 1H), 3.27–3.31 (m, 2H), 2.70–2.88 (m, 1H), 2.31 (s, 1H), 2.20–2.31 (m, 2H), 1.89–1.93 (m, 1H), 1.64–1.77 (m, 3H), 1.13 (t, $J = 7.2$ Hz, 3H); ^{13}C NMR (75 MHz, $CDCl_3$) δ 167.00, 151.14, 142.78, 139.02, 136.11 (2C), 135.57, 134.39, 132.38, 129.02, 128.40 (2C), 127.65 (2C), 126.26 (2C), 122.66, 122.12, 119.97, 109.19, 62.33, 53.58, 48.15, 46.77, 40.89, 30.30, 28.30, 23.00, 14.16; HRMS (ESI$^+$): m/z: calcd for $C_{29}H_{31}Cl_2N_4O$ 521.1797 [M+H]$^+$; found: 521.1795.

*4.1.3.2. 4-((2-(2,6-Dichlorobenzyl)-1H-benzo[d]imidazol-1-yl) methyl)eN-(1-methylpiperidin-4-yl)benzamide (**37**).* Following the general procedure for compounds **36**–**44**, 4-((2-(2,6-dichlorobenzyl)-1*H*-benzo[*d*]imidazol-1-yl)methyl)benzoic acid **35** (50 mg, 0.12 mmol), oxalyl chloride (20 μL, 0.24 mmol), 1-methylpiperidin-4-amine (15 μL, 0.13 mmol), and DIPEA (43 μL, 0.30 mmol) gave the title product **37** as a white solid (50 mg, 40%); $R_f = 0.40$ (CH_2Cl_2/MeOH: 10/1); mp: 175.2–177.4 °C; HPLC purity: 10.09 min, 98.2%; ^{1}H NMR (400 MHz, DMSO-d_6) δ 8.23 (d, $J = 4.0$ Hz, 1H),7.83 (d, $J = 8.4$ Hz, 2H), 7.48–7.54 (m, 4H), 7.39 (t, $J = 8.4$ Hz, 1H), 7.27 (d, $J = 8.0$ Hz, 2H), 7.13–7.20 (m, 2H), 5.73 (s, 2H), 4.50 (s, 2H), 3.73 (quintet, $J = 3.6$ Hz, 1H), 2.80 (d, $J = 11.6$ Hz, 2H), 2.20 (s, 3H), 2.01 (t, $J = 11.2$ Hz, 2H), 1.76 (d, $J = 10.8$ Hz, 2H), 1.59 (qd, $J = 11.6$ Hz, 2.4 Hz, 2H); ^{13}C NMR (101 MHz, DMSO-d_6) δ 165.72, 151.65, 142.65, 140.21, 135.89 (2C), 134.53, 133.47, 129.99, 128.82 (2C), 128.26 (2C), 126.95 (2C), 122.56, 122.03, 121.99, 119.25, 110.60, 54.80 (2C), 46.81, 46.42, 46.19, 31.69 (2C), 30.28; HRMS (ESI$^+$): m/z: calcd for $C_{28}H_{29}Cl_2N_4O$ 507.1640 [M+H]$^+$; found: 507.1642.

*4.1.3.3. 4-((2-(2,6-Dichlorobenzyl)-1H-benzo[d]imidazol-1-yl) methyl)eN-(3-(dimethylamino)propyl)benzamide (**38**).* Following the general procedure for compounds **36**–**44**, 4-((2-(2,6-dichlorobenzyl)-1*H*-benzo[*d*]imidazol-1-yl)methyl)benzoic acid **35** (50 mg, 0.12 mmol), oxalyl chloride (20 μL, 0.24 mmol), N^1,N^1-dimethylpropane-1,3-diamine (16 μL, 0.13 mmol), and DIPEA (43 μL, 0.30 mmol) gave the title product **38** as a white solid (60 mg, 48%); $R_f = 0.20$ (CH_2Cl_2/MeOH: 10/1); mp: 235.6–237.5 °C; HPLC purity: 6.37 min, 98.9%; ^{1}H NMR (400 MHz, MeOD) δ 7.84 (d, $J = 8.0$ Hz, 2H), 7.58 (dd, $J = 6.4$ Hz, 2.8 Hz, 1H), 7.44–7.46 (m, 3H), 7.25–7.35 (m, 5H), 5.74 (s, 2H), 4.58 (s, 2H), 3.49 (t, $J = 6.4$ Hz, 2H), 3.18 (t, $J = 7.6$ Hz, 2H), 2.92 (s, 6H), 2.03 (quintet, $J = 7.2$ Hz, 2H); ^{13}C NMR (75 MHz, MeOD) δ 168.38, 151.63, 141.66, 140.00, 135.99 (2C), 135.28, 133.54, 132.05, 129.22, 128.20 (2C), 127.56 (2C), 126.35 (2C), 122.72, 122.12, 118.14, 109.63, 56.09, 46.07, 43.09 (2C), 37.04, 29.60, 25.78; HRMS (ESI$^+$): m/z: calcd for $C_{27}H_{29}Cl_2N_4O$ 495.1713 [M+H]$^+$; found: 495.1694.

*4.1.3.4. 4-((2-(2,6-Dichlorobenzyl)-1H-benzo[d]imidazol-1-yl) methyl)eN-(3-(pyrrolidin-1-yl)propyl)benzamide (**39**).* Following the general procedure for compounds **36**–**44**, 4-((2-(2,6-dichlorobenzyl)-1*H*-benzo[*d*]imidazol-1-yl)methyl)benzoic acid **35** (50 mg, 0.12 mmol), oxalyl chloride (20 μL, 0.24 mmol), 3-(pyrrolidin-1-yl)propan-1-amine (35 μL, 0.27 mmol) and DIPEA (43 μL, 0.30 mmol) gave the title product **39** as a white solid (47 mg, 74%); $R_f = 0.30$ (CH_2Cl_2/MeOH: 10/1); mp: 218.0–220.2 °C; HPLC purity: 7.48 min, 99.7%; ^{1}H NMR (300 MHz, $CDCl_3$ with MeOD) δ 7.80 (d, $J = 8.4$ Hz, 2H), 7.68–7.69 (m, 1H), 7.31–7.38 (m, 2H overlapped with $CDCl_3$ peak), 7.24–7.27 (m, 4H), 7.17–7.22 (m, 3H), 5.55 (s, 2H), 4.50 (s, 2H), 3.51 (t, $J = 6.3$ Hz, 2H), 3.38–3.40 (m, 4H), 3.17 (t, $J = 7.2$ Hz, 2H), 2.03–2.11 (m, 6H); ^{13}C NMR (75 MHz, DMSO-d_6) δ 166.55, 151.64, 142.66, 140.44, 135.88 (2C), 134.19, 133.14, 133.45, 129.97, 128.80 (2C), 128.16 (2C), 127.06 (2C), 122.57, 122.00, 119.27, 110.57, 53.71 (2C), 52.57, 46.40, 37.00, 30.26, 26.44, 23.08 (2C); HRMS (ESI$^+$): m/z: calcd for $C_{29}H_{31}Cl_2N_4O$ 521.1869 [M+H]$^+$; found: 521.1865.

*4.1.3.5. 4-((2-(2,6-Dichlorobenzyl)-1H-benzo[d]imidazol-1-yl) methyl)eN-(3-(4-methylpiperazin-1-yl)propyl)benzamide (**40**).* Following the general procedure for compounds **36**–**44**, 4-((2-(2,6-dichlorobenzyl)-1*H*-benzo[*d*]imidazol-1-yl)methyl)benzoic acid **35** (50 mg, 0.12 mmol), oxalyl chloride (20 μL, 0.24 mmol), 3-(4-methylpiperazin-1-yl)propan-1-amine (30 μL, 0.27 mmol), and

DIPEA (43 μL, 0.30 mmol) gave the title product **40** as a white solid (50 mg, 75%); R_f = 0.25 (CH_2Cl_2/MeOH: 10/1); mp: 209.8–212.1 °C; HPLC purity: 6.99 min, 96.3%; ^{1}H NMR (300 MHz, DMSO-d_6) δ 8.49 (br t, J = 4.8 Hz, 1H), 7.80 (d, J = 8.1 Hz, 2H), 7.50 (d, J = 8.1 Hz, 4H), 7.35–7.37 (m, 1H), 7.24–7.28 (m, 2H), 7.14–7.16 (m, 2H), 5.72 (s, 2H), 4.48 (s, 2H), 3.39 (m, 2H), 3.10–3.21 (m, 8H overlapped with H_2O peak), 2.37–2.41 (m, 2H overlapped with DMSO-d_6 peak), 2.29 (s, 3H), 1.66 (t, J = 6.9 Hz, 2H); ^{13}C NMR (101 MHz, DMSO-d_6) δ 166.26, 151.65, 142.61, 140.24, 135.87 (2C), 134.39, 133.42, 129.95, 128.94, 128.78 (2C), 128.09 (2C), 127.02 (2C), 122.59, 122.00, 119.23, 110.56, 55.55, 54.12 (2C), 51.86 (2C), 46.36, 44.88, 38.11, 30.24, 26.30; HRMS (ESI$^+$): m/z: calcd for $C_{30}H_{34}Cl_2N_5O$ 550.2135 [M+H]$^+$; found: 550.2132.

*4.1.3.6. 4-((2-(2,6-Dichlorobenzyl)-1H-benzo[d]imidazol-1-yl) methyl)eN-(3-(piperidin-1-yl)propyl)benzamide (**41**).* Following the general procedure for compounds **36**–**44**, 4-((2-(2,6-dichlorobenzyl)-1*H*-benzo[*d*]imidazol-1-yl)methyl)benzoic acid **35** (50 mg, 0.12 mmol), oxalyl chloride (20 μL, 0.24 mmol), 3-(4-methylpiperazin-1-yl)propan-1-amine (34 μL, 0.27 mmol), and DIPEA (43 μL, 0.30 mmol) gave the title product **41** as a white solid (40 mg, 61%); R_f = 0.35 (CH_2Cl_2/MeOH: 10/1); mp: 149.1–153.9 °C; HPLC purity: 11.92 min, 99.8%; ^{1}H NMR (300 MHz, MeOD) δ 7.82 (dd, J = 8.4 Hz, 1.8 Hz, 2H), 7.56–7.59 (m, 1H), 7.42–7.45 (m, 3H), 7.23–7.32 (m, 5H), 5.72 (s, 2H), 4.56 (s, 2H), 3.48 (t, J = 6.6 Hz, 2H), 3.15 (m, 2H), 3.07 (t, J = 7.8 Hz, 4H), 3.06 (q, J = 7.8 Hz, 2H), 1.84 (t, J = 7.8 Hz, 4H) 1.31 (m, 2H); ^{13}C NMR (101 MHz, Acetone-d_6) δ 168.70, 151.22, 142.98, 141.04, 136.00 (2C), 135.83, 133.38, 132.85, 129.22, 128.22 (2C), 127.96 (2C), 126.75 (2C), 122.18, 121.62, 119.13, 109.70, 54.01, 53.14 (2C), 46.20, 36.11, 29.90, 24.60, 23.50 (2C), 21.76; HRMS (ESI$^+$): m/z: calcd for $C_{30}H_{33}Cl_2N_4O$ 535.1953 [M+H]$^+$; found: 535.1954.

*4.1.3.7. 4-((2-(2,6-Dichlorobenzyl)-1H-benzo[d]imidazol-1-yl) methyl)eN-(3-(piperidin-1-yl)ethyl)benzamide (**42**).* Following the general procedure for compounds **36**–**44**, 4-((2-(2,6-dichlorobenzyl)-1*H*-benzo[*d*]imidazol-1-yl)methyl)benzoic acid **35** (50 mg, 0.12 mmol), oxalyl chloride (20 μL, 0.24 mmol), 3-(4-methylpiperazin-1-yl)ethan-1-amine (38 μL, 0.27 mmol), and DIPEA (43 μL, 0.30 mmol) gave the title product **42** as a white solid (37 mg, 54%); R_f = 0.30 (CH_2Cl_2/MeOH: 10/1); mp: 240.4–242.1 °C; HPLC purity: 11.92 min, 99.8%; ^{1}H NMR (400 MHz, DMSO-d_6) δ 8.68 (br t, J = 5.6 Hz, 1H), 7.85 (d, J = 8.0 Hz, 2H), 7.49–7.54 (m, 4H), 7.38–7.42 (m, 1H), 7.31 (d, J = 8.0 Hz, 2H), 7.13–7.21 (m, 2H), 5.75 (s, 2H), 4.50 (s, 2H), 3.60 (q, J = 5.6 Hz, 2H), 3.52 (m, 2H), 3.21 (m, 2H), 2.93 (m, 2H), 1.81 (m, 2H), 1.67 (m, 3H), 1.41 (m, 2H); ^{13}C NMR (101 MHz, DMSO-d_6) δ 167.03, 153.02, 151.64, 142.65, 140.82, 135.86 (2C), 133.42, 130.01, 128.82 (2C), 128.28 (2C), 127.14 (2C), 122.57, 122.14, 122.01, 119.29, 110.56, 52.79 (2C), 46.40 (2C), 30.42, 29.94, 23.00 (2C), 21.85; HRMS (ESI$^+$): m/z: calcd for $C_{29}H_{31}Cl_2N_4O$ 521.1869 [M+H]$^+$; found: 521.1866.

*4.1.3.8. 4-((2-(2,6-Dichlorobenzyl)-1H-benzo[d]imidazol-1-yl) methyl)eN-(3-morpholinopropyl)benzamide (**43**).* Following the general procedure for compounds **36**–**44**, 4-((2-(2,6-dichlorobenzyl)-1*H*-benzo[*d*]imidazol-1-yl)methyl)benzoic acid **35** (50 mg, 0.12 mmol), oxalyl chloride (20 μL, 0.24 mmol), 3-morpholinopropan-1-amine (39 μL, 0.27 mmol), and DIPEA (43 μL, 0.30 mmol) gave the title product **43** as a white solid (40 mg, 65%); R_f = 0.30 (CH_2Cl_2/MeOH: 10/1); mp: 190.3–193.2 °C; HPLC purity: 8.29 min, 99.8%; ^{1}H NMR (300 MHz, $CDCl_3$) δ 8.09 (t, J = 4.5 Hz, 1H), 7.72–7.78 (m, 3H), 7.20–7.31 (m, 5H), 7.12–7.18 (m, 3H), 5.51 (s, 2H), 4.47 (s, 2H), 3.68 (t, J = 8.4 Hz, 4H), 3.55 (t, J = 8.4 Hz, 2H), 2.20–2.40 (m, 6H), 1.80 (q, J = 8.4 Hz, 2H); ^{13}C NMR (75 MHz, $CDCl_3$) δ 166.56, 162.57, 151.13, 142.69, 138.95, 136.07, 135.52, 134.46, 132.31, 129.07, 128.40 (2C), 127.72 (2C), 126.22 (2C), 122.72, 122.18, 119.88, 109.22, 67.00 (2C), 58.47, 53.81 (2C), 46.78, 40.42, 30.27, 24.40; HRMS (ESI$^+$): m/z: calcd for $C_{29}H_{31}Cl_2N_4O_2$ 537.1818 [M+H]$^+$; found: 537.1816.

*4.1.3.9. 4-((2-(2,6-Dichlorobenzyl)-1H-benzo[d]imidazol-1-yl) methyl)-N,N-dimethylbenzamide (**44**).* Following the general procedure for compounds **36**–**44**, 4-((2-(2,6-dichlorobenzyl)-1*H*-benzo[*d*]imidazol-1-yl)methyl)benzoic acid **35** (50 mg, 0.12 mmol), oxalyl chloride (20 μL, 0.24 mmol), dimethylamine hydrochloride (24 mg, 0.30 mmol), and DIPEA (43 μL, 0.30 mmol) gave the title product **44** as a white solid (23 mg, 42%); R_f = 0.30 (CH_2Cl_2/MeOH: 10/1); mp: 225.7–228.2 °C; HPLC purity: 9.91 min, 99.7%; ^{1}H NMR (400 MHz, MeOD) δ 7.87 (dd, J = 6.4 Hz, 3.2 Hz, 1H), 7.75–7.77 (m, 1H), 7.64–7.67 (m, 2H), 7.54 (d, J = 8.4 Hz, 2H), 7.41–7.48 (m, 3H), 7.34 (d, J = 8.4 Hz, 2H), 5.95 (s, 2H), 5.03 (s, 2H), 3.10 (s, 3H), 2.98 (s, 3H); ^{13}C NMR (101 MHz, Acetone-d_6) δ 169.75, 151.35, 137.42, 136.30, 134.51, 132.87, 131.67, 130.46, 129.24 (2C), 127.97, 127.90 (2C), 127.09 (2C), 127.06 (2C), 126.93, 114.38, 113.08, 48.36 (2C), 38.59, 34.28; HRMS (ESI$^+$): m/z: calcd for $C_{24}H_{22}Cl_2N_3O$ 438.1134 [M+H]$^+$; found: 438.1133.

*4.1.4. General procedure for the synthesis of compound **51**–**53***

To a stirred solution of 4-((2-(2-(5-isopropyl-2-methylphenylamino)-2-oxoethyl)-1*H*-benzo[*d*]imidazol-1-yl) methyl)benzoic acid **50** (1.0 equiv), Et_3N (1.2 equiv), and benzotriazole-1-yl-oxy-tris-(dimethylamino)-phosphonium hexafluorophosphate (BOP; 2.0 equiv) in DMF was added the desired substituted amine (1.2 equiv). After stirring for 12–16 h at room temperature, the reaction mixture was concentrated in vacuo, and extracted with EtOAc (3 × 30 mL). The organic layer was dried over anhydrous $MgSO_4$, filtered, concentrated, and purified by column chromatography on SiO_2 (CH_2Cl_2/MeOH: 10/1).

*4.1.4.1. N-((1-Ethylpyrrolidin-2-yl)methyl)-4-((2-(2-(5-isopropyl-2-methylphenylamino)-2-oxoethyl)-1H-benzo[d]imidazol-1-yl)methyl) benzamide (**51**).* Following the general procedure for compounds **51**–**53**, 4-((2-(2-(5-isopropyl-2-methylphenylamino)-2-oxoethyl)-1*H*-benzo[*d*]imidazol-1-yl)methyl)benzoic acid **50** (40 mg, 0.09 mmol), BOP (80 mg, 0.18 mmol), Et_3N (25 μL, 0.18 mmol), and (1-ethylpyrrolidin-2-yl)methanamine (14 μL, 0.10 mmol) in DMF (4 mL) gave the title product **51** as a white solid (40 mg, 80%) R_f = 0.15 (CH_2Cl_2/MeOH: 10/1); mp: 174.0–175.9 °C; HPLC purity: 16.17 min, 95.3%; ^{1}H NMR (300 MHz, $CDCl_3$) δ 10.53 (br s, 1H), 8.07 (s, 1H), 7.73–7.79 (m, 4H), 7.27–7.31 (m, 3H), 7.06–7.09 (m, 3H), 6.91 (d, J = 7.5 Hz, 1H), 5.47 (s, 2H), 3.96 (s, 2H), 3.67–3.72 (m, 4H), 3.32–3.35 (m, 1H), 3.02–3.07 (m, 2H), 2.81 (m, 1H), 2.29 (s, 3H), 2.19–2.22 (m, 2H), 2.01–2.07 (m, 2H), 1.90 (s, 2H), 1.20 (s, 3H), 1.18 (s, 3H); ^{13}C NMR (75 MHz, $CDCl_3$) δ 170.90, 164.78, 162.33, 149.25, 147.40, 141.71, 140.42, 135.77, 134.97, 131.35, 130.45, 128.46, 127.07, 126.71, 123.60, 123.20, 123.02, 121.05, 119.26, 109.94, 69.03, 53.59, 50.76, 46.64, 41.62, 35.24, 33.77, 26.38, 23.99 (2C), 23.57, 17.74, 11.34; HRMS (ESI$^+$): m/z: calcd for $C_{34}H_{42}N_5O_2$ 552.3333 [M+H]$^+$; found: 552.3333.

*4.1.4.2. N-(3-(Dimethylamino)propyl)-4-((2-(2-(5-isopropyl-2-methylphenylamino)-2-oxoethyl)-1H-benzo[d]imidazol-1-yl)methyl) benzamide (**52**).* Following the general procedure for compounds **51**–**53**, 4-((2-(2-(5-isopropyl-2-methylphenylamino)-2-oxoethyl)-1*H*-benzo[*d*]imidazol-1-yl)methyl)benzoic acid **50** (40 mg, 0.09 mmol), BOP (80 mg, 0.18 mmol), Et_3N (25 μL, 0.18 mmol), and N^1,N^1-dimethylpropane-1,3-diamine (10 μL, 0.10 mmol) in DMF (4 mL) gave the title product **52** as a white solid (15 mg, 50%) R_f = 0.20 (CH_2Cl_2/MeOH: 10/1); mp: 171.9–173.6 °C; HPLC purity: 7.98 min, 99.1%; ^{1}H NMR (300 MHz, DMSO-d_6) δ 9.92 (s, 1H), 8.48 (t,

$J = 5.7$ Hz, 1H), 7.77 (d, $J = 8.4$ Hz, 2H), 7.63 (dd, $J = 7.5$ Hz, 1.8 Hz, 1H), 7.36 (dd, $J = 6.0$ Hz, 1.5 Hz, 1H), 7.21–7.26 (m, 3H), 7.15–7.18 (m, 2H), 7.12 (m, 1H), 6.95–6.97 (m, 1H), 5.64 (s, 2H), 4.14 (s, 2H), 3.23–3.28 (m, 2H), 2.75–2.82 (septet, $J = 6.9$ Hz, 1H), 2.36 (m, 2H), 2.11–2.23 (m, 9H), 1.62–1.67 (quintet, $J = 6.9$ Hz, 2H), 1.14 (d, $J = 6.9$ Hz, 6H); ^{13}C NMR (75 MHz, DMSO-d_6) δ 166.50, 166.26, 162.34, 150.52, 146.75, 142.37, 140.14, 136.12, 135.39, 134.08, 130.69, 129.26, 127.91 (2C), 127.10 (2C), 123.04, 122.89, 122.47, 119.12, 56.88, 47.02, 44.95 (2C), 38.00, 33.38, 26.81, 24.26 (2C), 17.75, 13.11; HRMS (ESI$^+$): *m/z*: calcd for $C_{32}H_{40}N_5O_2$ 526.3104 [M+H]$^+$; found: 526.3102.

*4.1.4.3. 4-((2-(2-(5-Isopropyl-2-methylphenylamino)-2-oxoethyl)-1H-benzo[d]imidazol-1-yl)methyl)eN-(3-(piperidin-1-yl)propyl)benzamide (**53**).* Following the general procedure for compounds **51**–**53**, 4-((2-(2-(5-isopropyl-2-methylphenylamino)-2-oxoethyl)-1*H*-benzo[*d*]imidazol-1-yl)methyl)benzoic acid **50** (40 mg, 0.09 mmol), BOP (80 mg, 0.18 mmol), Et_3N (25 μL, 0.18 mmol), and 3-(piperidin-1-yl)propan-1-amine (14 μL, 0.10 mmol) in DMF (4 mL) gave the title product **53** as a white solid (48 mg, 90%) $R_f = 0.20$ (CH_2Cl_2/MeOH: 10/1); mp: 181.7–182.5 °C; HPLC purity: 13.10 min, 95.9%; ^{1}H NMR (300 MHz, MeOD) δ 7.83 (d, $J = 8.1$ Hz, 2H), 7.76 (d, $J = 8.1$ Hz, 1H), 7.35–7.43 (m, 5H), 7.20 (s, 1H), 7.14 (d, $J = 8.1$ Hz, 1H), 7.02 (d, $J = 8.1$ Hz, 1H), 5.79 (s, 2H), 4.48 (s, 2H), 3.45–3.52 (m, 4H), 3.13 (t, $J = 8.1$ Hz, 2H), 2.85–2.89 (m, 2H), 2.20 (s, 3H), 1.98–2.03 (m, 4H), 1.76–1.81 (m, 2H), 1.43 (m, 1H), 1.26–1.28 (m, 1H), 1.21 (s, 3H), 1.19 (s, 3H); ^{13}C NMR (75 MHz, MeOD) δ 168.79, 149.34, 147.05, 139.40, 134.91, 134.15, 133.35, 130.16 (2C), 129.77, 127.69 (2C), 126.70 (2C), 124.29 (2C), 123.86, 123.23, 117.19, 111.02, 54.31, 52.92 (2C), 48.16, 46.74 (overlapped with MeOD peaks), 36.31, 33.47, 24.14, 22.97 (3C), 22.94, 21.25, 16.24; HRMS (ESI$^+$): *m/z*: calcd for $C_{35}H_{44}N_5O_2$ 566.3417 [M+H]$^+$; found: 566.3415.

4.2. Cell-based assays

4.2.1. Cell culture

HT-22 (mouse hippocampal cells) cells were grown in Dulbecco's Modified Eagle's Medium (DMEM, GIBCO) supplemented with 10% (vol/vol) FBS and antibiotics (100 mg/mL penicillin/streptomycin mix) in a humidified atmosphere at 37 °C with 5% CO_2.

4.2.2. Preparation of $A\beta_{1-42}$

$A\beta_{1-42}$ (American Peptide) was suspended in 1 mL of 1,1,1,3,3,3 hexafluoro-2-propanol (HFIP; Sigma–Aldrich) using a gastight syringe. Peptide samples were vortexed to obtain a homogenous solution, aliquoted into microcentrifuge tubes and lyophilized. Protein amount for each batch was determined by BCA protein assay. The dried peptide films were stored desiccated at −80 °C. Aβ monomer solutions were prepared immediately before use to avoid possible aggregation. For each biological experiment, peptide films were resuspended to 5 mM in anhydrous dimethyl sulfoxide (DMSO).

4.2.3. JC-1 assay

HT-22 (mouse hippocampal cells) cells were cultured in Dulbecco's Modified Eagle's Medium (DMEM, GIBCO) supplemented with 100 μg/mL penicillin/streptomycin mixture and 10% (vol/vol) fetal bovine serum (FBS) in a humidified atmosphere at 37 °C with 5% CO_2. The cells were seeded into a clear 96-well plate (FALCON) in a number of 30,000 per well 24 h prior to the assay. JC-1 dye (Stratagene, USA) was diluted with phenol red-free Opti-MEM (GIBCO) medium to a concentration of 7.5 μM. The medium was removed from the plate, and 100 μL of JC-1 solution was added per well. After incubation for 1 h and 15 min at 37 °C, wells were washed twice with 100 μL of phosphate buffer solution (PBS). The cells were treated with test compounds in a concentration of 5 μM per well and incubated at 37 °C for 10 min. Then, for each test compound, three wells were treated with 5 μM of $A\beta_{1-42}$, and other two wells were treated with 5 μM of DMSO as vehicle control. The fluorescence intensity was measured at every 1 h for 3 h by using a microplate reader (Flexstation® 3, Molecular Devices, USA) reader at ex/em 485 nm/535 nm (green) and ex/em 560 nm/595 nm (red). The ratio of green to red fluorescence was calculated and normalized by taking the percent changes using vehicle control as 100%.

4.2.4. Luciferase-based ATP assay

To a clear 96-well plate, HT-22 cells were seeded in a number of 7000 per well one day prior to the assay. After removing the medium from the plate, four wells were treated with 25 μL/well of each test compound (5 μM). And the cells were incubated for 10 min at 37 °C. For each test compound, two wells were treated with 25 μL of Aβ solution (5 μM, American peptide, 1–42) and the other two wells were treated with 25 μL of DMSO solution (5 μM) as vehicle controls. Then, the cells were incubated for 7 h at 37 °C. After the incubation, the test compound-treated wells were washed twice with PBS, and lysed with 1% Triron-X 100 in TSBT buffer solution. To measure the protein concentrations of each well, BCA protein determination kit (Thermo scientific) was used. And the same amount of cell lysate was taken from each well and plated into a white 96-well plate (NUNC). And the ATP levels in each sample were measured by ATP determination kit (Molecular Probes, USA) containing D-luciferin and luciferase. The % inhibition value was measured by luminescence from detecting ATP levels from a microplate reader (Flexstation® 3, Molecular Devices, USA), and the result was normalized by taking the vehicle control as 0%. Cell viability (%) in each test compound was also determined by detecting the ATP levels of each well containing only each test compound (5 μM) and the cells.

4.2.5. MTT assay

To a clear 96-well plate, HT-22 cells were seeded in a number of 5000 per well as above described method for the ATP detection assay. After incubating the cells for 24 h at 37 °C, 10 μL of MTT solution (3-(4,5-dimethylthiazol-2-yl)-2,5-diphenyltetrazolium bromide, Sigma-Aldrich) was directly added to each well. The cells were incubated for 2 h at 37 °C. And 135 μL of MTT solubilizing solution (10% Triton-X 100 in isopropanol with 0.1 M HCl) was added to each well followed by additional incubation of the cells for 2 h at 37 °C. The % inhibition value was measured by the optical density (OD) values of absorbance at 560 nm and normalized by taking the vehicle control as 0%. Cell viability (%) was also determined by using OD values of each well containing only each test compound (5 μM) and the cells.

4.2.6. CM-H_2DCFDA-fluorescent ROS assay

To a black 96-well plate with clear bottom, HT-22 cells were seeded in a number of 10,000 per well and treated with 25 μL/well of each test compound (5 μM) and 25 μL/well of Aβ solution (5 μM) After incubating for 6 h at 37 °C, compound-treated wells were washed twice with HBSS. And 100 μL of 1 μM CM-H_2DCFDA (Invitrogen, C6827) in HBSS solution was directly added to each well. The cells were incubated for 30 min at 37 °C and washed twice with HBSS. The total fluorescent intensity from each well was measured by using a high-content imaging system (Operetta, Perkin Elmer). The % inhibition of Aβ-induced ROS production was determined by calculating % ratio of the increased fluorescent intensity from the test compound-treated wells to untreated wells in the presence of the Aβ solution.

4.2.7. Measurement of intracellular Ca^{2+} level

To a black 96-well plate with clear bottom, HT-22 cells were seeded in a number of 10,000 per well. And 25 μL/well of Aβ solution (5 μM), 25 μL/well of each test compound, and 100 μL/well of intracellular Ca^{2+} indicating dye (5 μM), Fura-2 AM (Molecular Probes), in phenol red-free medium was added. After incubating the cells for 30 min at 37 °C, each well was washed twice with 100 μL/well of HBSS. And the plate was incubated for 30 min to allow complete deesterification of intracellular AM esters. Then, fluorescence was measured by a microplate reader (Flexstation® 3, Molecular Devices, USA) at excitation and emission wavelengths (ex/em) of 380 nm/340 nm. The intracellular Ca^{2+} level was determined by calculating % ratio of the increased fluorescent intensity from the test compound-treated wells to untreated wells in the presence of the Aβ solution (control).

4.2.8. CYP inhibition assay

Inhibitions of CYP (CYP1A2, 2C9, 2D6, 2C19, and 3A4) activities were measured using the Vivid® CYP450 screening kit (Invitrogen, Madison, WI, USA) in a clear 96-well plate. Positive controls including the α-naphthoflavone (CYP1A2), sulfaphenazole (CYP2C9), quinidine (CYP2D6), miconazol (CYP2C19), and ketoconazole (CYP3A4) were prepared as 10 mM solution in MeCN. And then, each sample (test compounds, positive inhibition control and solvent control) and the Master Pre-Mix [CYP450 BACULOSOMES® Reagent (recombinant human CYP450 isozyme and rabbit NADPHP450 reductase) and Regeneration System (3.3 mM glucose-6-phosphate and 0.3 U/ml glucose-6-phosphate dehydrogenase in 100 mM potassium phosphate, pH 8.0)] were added to each well. After incubating the mixture for 5 min at 37 °C, the Vivid® CYP substrates and 0.1 mM NADP+ buffer was added to begin the enzyme reaction. The remaining enzyme activity (% remaining activity) was measured after 20 min by using a fluorescent plate reader.

4.2.9. hERG inhibition assay

For automated patch-clamp NPC-16 Patchliner (Nanion Technologies, München, Germany) recordings, CHO-K1 Tet-On hERG cells (IonGate Biosciences GmbH, Frankfurt, Germany) were plated into the 100-mm culture dishes. Whole-cell currents were recorded with the intracellular solution containing: 50 mM KCl, 60 mM kF, 10 mM NaCl, 2 mM $MgCl_2$, 20 mM EGTA and 10 mM HEPES (pH 7.2), and with the extracellular solution containing: 140 mM NaCl, 4 mM KCl, 2 mM $CaCl_2$, 1 mM $MgCl_2$, 5 mM Glucose and 10 HEPES (pH 7.4). To assist stable seal formations, the seal enhancer containing: 80 mM NaCl, 3 mM KCl, 35 mM $CaCl_2$, 10 mM $MgCl_2$ and 10 mM HEPES (pH 7.4) was used only at the seal formation step. Prior to the whole-cell recordings, the external seal enhancing solution was exchanged to the extracellular solution described above. hERG channel currents were recorded using the parallel EPC-10 patch-clamp amplifiers (HEKA Elektronik, Lambrecht/Pfalz, Germany), and low-pass filtered (10 kHz) with a 4-pole Bessel filter. Cell suspension and patch solutions were automatically added onto the four recording wells in the microfabricated disposable chip (NPC-16 Chip, Nanion Technologies, München, Germany). To obtain the inhibitory constants, hERG tail currents were evoked by repolarizing steps to −50 mV for 500 ms preceded by a 500-ms depolarization potential of +20 mV at a holding potential of −80 mV with a 20-s sweep interval. Whole-cell currents were acquired and digitized at 5 kHz using Patchmaster (HEKA Elektronik, Lambrecht/Pfalz, Germany). The extracellular solution was exchanged to the extracellular solution containing each blocker *via* four pipette tips of NPC-16 Patchliner using a 4-fold volume of solution (40 μL) with a speed of 4 μL/s, and the exchanged blocker solution was applied for 100–200 s to the patch-clamped cells until blocker binding had reached equilibrium by monitoring hERG tail currents. Whole-cell recordings were analyzed using the Patchmaster/Fitmaster (HEKA Elektronik, Lambrecht/Pfalz, Germany), IGOR Pro (WaveMetrics Inc., Portland, OR, USA), and the GraphPad Prism 4.0 (GraphPad Software, Inc., La Jolla, CA, USA) software.

4.3. Pharmacokinetic study

4.3.1. Animals

Male SD rats (Nara Biotech, Korea), 8-week old, were used in the experiments. Animals were housed under a 12-h light-dark cycle, with food and water *ad libitum*. Rats were allowed to be accustomed to the environment for at least 1 week prior to their usage in the experiments. All animal handling was in accordance with guidelines of the Animal Care and Use Committee in Korea Institute of Science and Technology. The rats were studied after anesthesia induced by intraperitoneal injection of isoflurane.

4.3.2. Drug preparation and administration

Compounds were dissolved completely at 10 mg/2 mL of *N*-Methyl-2-pyrrolidone, tween80, and D.W. (1:2:7 by volume) by sonication for 5 min. This preparation was orally administered at 2 mL/kg with a blunt needle *via* the esophagus into the stomach.

Blood samples were collected from heart puncture by using a syringe with heparinized needle at 30 m, 3 h ($n = 5$) after drug administration. The blood samples were centrifuged for 5 min at 10,000×*g*, and the plasma samples were stored at −70 °C until LC-MS/MS analysis. After collection of blood samples, brain were extracted (n = 5, per sampling time). All extracted tissues were blot dried, weighed and homogenized (Ultra-Turrax®, T25 basic, IKA Labortechnic, Malasia) with 4 times its volume of distilled water. Obtained tissue homogenates were kept at −70 °C until LC-MS/MS analysis.

4.3.3. Sample preparation

To determine the drug concentration in the plasma, 50 μL of the plasma sample was mixed with 100 μL carbamazepine (0.1 μg/mL in acetonitrile, internal standard) and vortexed for 30 s. The mixture was centrifuged for 10 min at 10,000×*g* and 100 μL supernatant was analyzed by LC-MS/MS.

To determine the drug concentration in the brain, 100 μL of the brain sample was mixed with 200 μL carbamazepine (0.1 μg/mL in acetonitrile, internal standard) and vortexed for 30 s. The mixture was centrifuged for 10 min at 10,000×*g* and 100 μL supernatant was analyzed by LC-MS/MS.

4.3.4. LC-MS/MS analysis

The Agilent 1100Series (Agilent Technologies, Waldbronn, Germany) was used. Mass spectrometer API 3200 (Applied Biosystems Sciex, Rotterdam, The Netherlands) with electrospray-positive ionization was used. The multiple reaction monitor was set at 274.3–185.0 *m/z* for each compound and 237.4–194.4 *m/z* for the internal standard. The analytical column was Waters XTrerra® MS C18 (3.5 μm, 2.1 mm i.d. × 50 mm). The mobile phase of paclitaxel consisted of (A) containing 0.1% formic acid and (B) 90% acetonitrile containing 0.1% formic acid. 5 μL aliquots were injected, and the flow rate was set at 0.35 mL/min. The initial composition was 10% (B), programmed linearly to 90% (B) after 1 min, and held for 1 min. The column was then re-equilibrated at 10% for 3 min.

4.4. In vivo studies

4.4.1. Animals

The acute AD mice model was prepared by administration of $A\beta_{1-42}$ solution (10% DMSO/90% PBS) to male ICR mice (6 weeks

old, 30–33 g) *via* intracerebroventricular (ICV) injection ($A\beta_{1-42}$ dose: 500 pmol/mouse) as described previously [33]. The wild type mice (B6C3F1) and double APP/PS1 transgenic mice (Tg AD mice model; APPswe/PSEN1dE9) was purchased from Jackson Laboratory (Bar Harbor, Maine, USA). The Tg AD mice model was 11 months old at the beginning of the behavior test, and the mice were housed for 1 month in a room under controlled temperature and fed *ad libitum*. The behavior tests were conducted during daytime in air-controlled and soundproof experiment room. The animal experiments were abided by the guidelines of the Institutional Animal Care and Use Committee of Korea Institute of Science and Technology.

4.4.2. Y-maze spontaneous alternation test

To the acute AD mice model (n = 7 per group), each test compound (test compound in 20% cyclodextrin, 30 mg/kg) was intravenously injected daily for 6 days. The Y-maze spontaneous alternation test was performed 1 day after the administration of each test compound. The Y maze was made of three equally spaced black plastic arms (40 L × 10 W × 12 H cm) positioned at an equal angle. Each acute AD model mouse were placed at the end of one arm and allowed to move freely through the maze for 8 min, and the sequence of arm entries was recorded. The arm entry of the mouse was counted when the all four limbs were within an arm. A spontaneous alternation was considered as entry into all three arms. The spontaneous alternation (%) was calculated by the following equation:

$$\text{Spontaneous alternation (\%)} = 100 \times \{\text{number of alternations}/(\text{total number of arm entries} - 2)\}$$

4.4.3. Contextual fear conditioning test

To the Tg AD mice model (n = 7 per group), each test compound (30 mg/kg) was orally administrated daily for 1 month. Each mouse was placed in a fear-conditioning chamber (Courlbourn, USA) for 90 s before giving an electric shock. Trials of training were performed using the chamber equipped with a fear conditioning system (FreActimetrics, USA). The training was performed by giving a conditional stimulus (CS) of 75 dB sound for 20 s followed by an unconditional stimulus (US) of electric foot shock (0.5 mA) for the last 2 s in CS. After an additional stay for 1 min, the mouse was returned to its home cage. Fear conditioning test was conducted 24 h after the training. The mouse was placed in the same chamber for 5 min without presentation of CS. Freezing behavior was considered as the complete absence of any movement except for respiration and heartbeat. Freezing response was measured by the fear conditioning system without application of CS or US.

4.5. TSPO binding assay

A radioligand [^{3}H] PK11195 was purchased from PerkinElmer Life and Analytical Sciences (Waltham, MA, USA). Non-labeled PK11195 (Tocris, Bristol, UK) was used as reference materials. To obtain a membrane preparation for the 18 kDa TSPO binding assay, 200–250 g male SD rats were purchased from Koatech Animal Inc. (Pyeongtaek, Korea). All procedures involving animals were conducted in accordance with the guidelines of the Korea Food Research Institutional Animal Care and Use Committee (permission No.: KFRI-M-09118). The cerebral cortex from 4 male SD rats was homogenized for 10 s in 20 mL of Tris-HCl buffer (30 mM, pH 7.4). The suspension was centrifuged at 27,000×*g* for 10 min, and the pellet was washed 3 times with Tris-HCl buffer. The washed pellet was homogenized in 20 mL of Tris-HCl buffer, and the suspension was incubated in a water bath (37 °C) for 30 min. Next, the suspension was centrifuged at 27,000×*g* for 10 min. The final membrane pellet was resuspended in 30 mL of Tris-HCl buffer and stored in aliquots at −80 °C until it was used in the binding assay. The membrane preparation was thawed and washed with 20 mL of Tris-citrate buffer (50 mM, pH 7.1, 0–4 °C) 3 times. The pellet was resuspended at a final concentration of 2.5 μg protein in 100 μL binding buffer, and the suspension was used for the binding assay. A membrane suspension (180 μL) was added to 10 μL of a test solution and 10 μL of 1 nM (final concentration) [^{3}H] PK-11,195 in a 96-well plate. The solution was mixed and incubated for 60 min at 25 °C. The binding reaction was terminated by rapid filtration onto a Whatman GF/C glass fiber filter with ice-cold 30 mM Tris-HCl buffer to remove any unbound [^{3}H] PK-11195. The filters were dried at 60 °C for 30 min and suspended in Wallac microbeta plate scintillation fluid. The amount of filter-bound radioactivity was counted using a Wallac 1450 Microbeta liquid scintillation counter (PerkinElmer Life and Analytical Sciences, Waltham, MA, USA). Total binding and non-specific binding were determined using the binding buffer and non-labeled PK-11195 (1 μM, final concentration), respectively. The percent displacement of the radioligand binding was determined by the following equation:

$$\text{Binding displacement (\%)} = 100 \times \{1 - (\text{DPM}_{\text{sample}} - \text{DPM}_{\text{NSB}})/(\text{DPM}_{\text{TB}} - \text{DPM}_{\text{NSB}})\}$$

where DPM, TB, and NSB denote disintegrations per minute, total binding, and non-specific binding, respectively. IC_{50} values were calculated from the binding displacement curve, which was fitted to a one-site competition-binding model using the Prism 5.0 (GraphPad Software Inc., San Diego, CA, USA). Values of binding affinity (K_i) were calculated by the following equation:

$$K_i = \text{IC}_{50}/(1 + [L]/K_d)$$

where [L] denotes the concentration of [^{3}H] PK11195 used and K_d denotes the competitor-ligand dissociation equilibrium constant for [^{3}H] PK11195.

4.6. Surface plasmon resonance (SPR) measurements

SPR measurements were performed with Biacore T200 optical biosensor system equipped with CM5 sensor chips (GE Healthcare) at 25 °C. Recombinant protein of human TSPO (18 kDa, Origene Technologies, Inc., No.: TP320107) was covalently immobilized on a CM5 chip using standard amine-coupling protocols in 10 mM sodium acetate (pH 4.5) at a flow rate of 10 μL/min for 1500 s, to obtain densities of 4000–6000 response unit (RU). All of the tested compounds were dissolved in 100% DMSO to obtain 10 mM solutions, and serially diluted in PBS-P buffer (10 mM NaH_2PO_4, 150 mM NaCl, pH 7.4) to a final concentration of 1.0%. The filtered PBS-P buffer containing 1.0% DMSO was prepared for the running buffer. For each tested compounds, the SPR measurements were performed using a five-point concentration series, 0.01–5 μM. In each analysis, multiple blank samples of running buffer alone were included. Typically, a series of different concentrations were injected over the immobilized chip at a flow rate of 50 μL/min (contact time: 120 s, dissociation time: 300 s), followed by the regeneration phase at a flow rate of 50 μL/min (contact time: 120 s, stabilization time: 10 s). The K_D values of each tested compounds were determined by Biacore T200 evaluation software (GE Healthcare) after the standard solvent correction process.

4.7. Molecular docking

The homology model of three-dimensional (3D) human TSPO was built on the atomic coordinates of the X-ray crystal structure of bacterial TSPO (PDB ID: 4RYI) using Modeler9v7 program (Discovery Studio 4.0, Accelrys, San Diego, CA, USA). Glide software (Glide ver. 5.6; Schrödinger, LLC, NY, USA) was used to carry out protein preparation, ligand preparation (in pH 7.4) and calculation, and molecular docking studies. First, the glide, an enclosing box centered at PK-11195, was generated from the built homology model of human TSPO. Then, each docked ligand was prepared for the glide docking. By using Glide software in extra precision (XP) mode, the putative binding modes of compound **25** were generated. The glide docking score of compound **25** was compared to PK-11195, which was re-docked to the same binding site.

Acknowledgement

This work was supported by the National Research Council of Science & Technology (NST) grant by the Korea government (MSIP) (No. CRC-15-04-KIST) and KIST institutional program (2E26650). J.L. was supported by the Sungshin Women's University Research Grant of 2015-2-21-007.

Appendix A. Supplementary data

Supplementary data related to this article can be found at http://dx.doi.org/10.1016/j.ejmech.2016.11.017.

Abbreviations

Aβ	amyloid-β
AD	Alzheimer's disease
mPTP	mitochondrial permeability transition pore
TSPO	translocator protein
CsA	cyclosphorin A
CNS	central nervous system
NFT	neurofibrillary tangles
ER	endoplasmic reticulum
Cyp D	cyclophilin D
ROS	reactive oxygen species
ALS	amyotrophic lateral sclerosis
ANT	adenine nucleotide translocator
VDAC	voltage-dependent anion channel
PPA	polyphosphoric acid
FBS	fetal bovine serum
PBS	phosphate buffered saline
BSA	bovine serum albumin
ATP	adenine triphosphate
CYP450	cytochrome P450
hERG	human ether-a-go-go-related gene
BBB	blood brain barrier
HATU	1-[bis(dimethylamino)methylene]-1*H*-1,2,3-triazolo[4,5-*b*]pyridinium3-oxidhexafluoro-phosphate
DIPEA	diisopropylamine
TLC	thin layer chromatography

References

[1] G. Waldemar, B. Dubois, M. Emre, J. Georges, I.G. McKeith, M. Rossor, P. Scheltens, P. Tariska, B. Winblad, Efns, Recommendations for the diagnosis and management of Alzheimer's disease and other disorders associated with dementia: EFNS guideline, Eur. J. Neurol. 14 (1) (2007) e1–26.
[2] R.E. Tanzi, L. Bertram, Twenty years of the Alzheimer's disease amyloid hypothesis: a genetic perspective, Cell 120 (4) (2005) 545–555.
[3] J. Hardy, D.J. Selkoe, The amyloid hypothesis of Alzheimer's disease: progress and problems on the road to therapeutics, Science 297 (5580) (2002) 353–356.
[4] F.M. LaFerla, K.N. Green, S. Oddo, Intracellular amyloid-beta in Alzheimer's disease, Nat. Rev. Neurosci. 8 (7) (2007) 499–509.
[5] A. Eckert, K. Schmitt, J. Gotz, Mitochondrial dysfunction - the beginning of the end in Alzheimer's disease? Separate and synergistic modes of tau and amyloid-beta toxicity, Alzheimers Res. Ther. 3 (3) (2011).
[6] K. Leuner, W.E. Muller, A.S. Reichert, From mitochondrial dysfunction to amyloid beta formation: novel insights into the pathogenesis of Alzheimer's disease, Mol. Neurobiol. 46 (1) (2012) 186–193.
[7] K.N. Green, F.M. LaFerla, Linking calcium to A beta and Alzheimer's disease, Neuron 59 (2) (2008) 190–194.
[8] A.A. Starkov, F.M. Beal, Portal to Alzheimer's disease, Nat. Med. 14 (10) (2008) 1020–1021.
[9] H. Du, L. Guo, F. Fang, D. Chen, A.A. Sosunov, G.M. McKhann, Y.L. Yan, C.Y. Wang, H. Zhang, J.D. Molkentin, F.J. Gunn-Moore, J.P. Vonsattel, O. Arancio, J.X. Chen, S. Du Yan, Cyclophilin D deficiency attenuates mitochondrial and neuronal perturbation and ameliorates learning and memory in Alzheimer's disease, Nat. Med. 14 (10) (2008) 1097–1105.
[10] A.P. Halestrap, S.J. Clarke, S.A. Javadov, Mitochondrial permeability transition pore opening during myocardial reperfusion–a target for cardioprotection, Cardiovasc. Res. 61 (3) (2004) 372–385.
[11] L.J. Martin, B. Gertz, Y. Pan, A.C. Price, J.D. Molkentin, Q. Chang, The mitochondrial permeability transition pore in motor neurons: involvement in the pathobiology of ALS mice, Exp. Neurol. 218 (2) (2009) 333–346.
[12] L.J. Martin, The mitochondrial permeability transition pore: a molecular target for amyotrophic lateral sclerosis therapy, Bba-Mol Basis Dis. 1802 (1) (2010) 186–197.
[13] R.L. Veech, C.R. Valeri, T.B. VanItallie, The mitochondrial permeability transition pore provides a key to the diagnosis and treatment of traumatic brain injury, IUBMB Life 64 (2) (2012) 203–207.
[14] H. Du, S.S. Yan, Mitochondrial permeability transition pore in Alzheimer's disease: cyclophilin D and amyloid beta, Biochim. Biophys. Acta 1802 (1) (2010) 198–204.
[15] A. Vianello, V. Casolo, E. Petrussa, C. Peresson, S. Patui, A. Bertolini, S. Passamonti, E. Braidot, M. Zancani, The mitochondrial permeability transition pore (PTP) - an example of multiple molecular exaptation? Biochim. Biophys. Acta 1817 (11) (2012) 2072–2086.
[16] T. Miura, M. Tanno, The mPTP and its regulatory proteins: final common targets of signalling pathways for protection against necrosis, Cardiovasc. Res. 94 (2) (2012) 181–189.
[17] M. Crompton, S. Virji, V. Doyle, N. Johnson, J.M. Ward, The mitochondrial permeability transition pore, Biochem. Soc. Symp. 66 (1999) 167–179.
[18] L. Veenman, V. Papadopoulos, M. Gavish, Channel-like functions of the 18-kDa translocator protein (TSPO): regulation of apoptosis and steroidogenesis as part of the host-defense response, Curr. Pharm. Des. 13 (23) (2007) 2385–2405.
[19] D.R. Green, J.C. Reed, Mitochondria and apoptosis, Science 281 (5381) (1998) 1309–1312.
[20] K.M. Broekemeier, M.E. Dempsey, D.R. Pfeiffer, Cyclosporin A is a potent inhibitor of the inner membrane permeability transition in liver mitochondria, J. Biol. Chem. 264 (14) (1989) 7826–7830.
[21] S.J. Clarke, G.P. McStay, A.P. Halestrap, Sanglifehrin A acts as a potent inhibitor of the mitochondrial permeability transition and reperfusion injury of the heart by binding to cyclophilin-D at a different site from cyclosporin A, J. Biol. Chem. 277 (38) (2002) 34793–34799.
[22] P.J. Henderson, H.A. Lardy, Bongkrekic acid. An inhibitor of the adenine nucleotide translocase of mitochondria, J. Biol. Chem. 245 (6) (1970) 1319–1326.
[23] Y.S. Kim, S.H. Jung, B.G. Park, M.K. Ko, H.S. Jang, K. Choi, J.H. Baik, J. Lee, J.K. Lee, A.N. Pae, Y.S. Cho, S.J. Min, Synthesis and evaluation of oxime derivatives as modulators for amyloid beta-induced mitochondrial dysfunction, Eur. J. Med. Chem. 62 (2013) 71–83.
[24] A. Elkamhawy, J. Lee, B.G. Park, I. Park, A.N. Pae, E.J. Roh, Novel quinazoline-urea analogues as modulators for A beta-induced mitochondrial dysfunction: design, synthesis, and molecular docking study, Eur. J. Med. Chem. 84 (2014) 466–475.
[25] R. Rupprecht, V. Papadopoulos, G. Rammes, T.C. Baghai, J. Fan, N. Akula, G. Groyer, D. Adams, M. Schumacher, Translocator protein (18 kDa) (TSPO) as a therapeutic target for neurological and psychiatric disorders, Nat. Rev. Drug Discov. 9 (12) (2010) 971–988.
[26] M.K. Chen, T.R. Guilarte, Translocator protein 18 kDa (TSPO): molecular sensor of brain injury and repair, Pharmacol. Ther. 118 (1) (2008) 1–17.
[27] A.M. Barron, L.M. Garcia-Segura, D. Caruso, A. Jayaraman, J.W. Lee, R.C. Melcangi, C.J. Pike, Ligand for translocator protein reverses pathology in a mouse model of Alzheimer's disease, J. Neurosci. 33 (20) (2013) 8891–8897.
[28] T. Bordet, B. Buisson, M. Michaud, C. Drouot, P. Galea, P. Delaage, N.P. Akentieva, A.S. Evers, D.F. Covey, M.A. Ostuni, J.J. Lacapere, C. Massaad, M. Schumacher, E.M. Steidl, D. Maux, M. Delaage, C.E. Henderson, R.M. Pruss, Identification and characterization of cholest-4-en-3-one, oxime (TRO19622), a novel drug candidate for amyotrophic lateral sclerosis, J. Pharmacol. Exp. Ther. 322 (2) (2007) 709–720.
[29] T. Kim, A.N. Pae, Translocator protein (TSPO) ligands for the diagnosis or treatment of neurodegenerative diseases: a patent review (2010-2015; part 1), Expert Opin. Ther. Pat. (2016) 1–27.

[30] C. Beaulieu, Z. Wang, D. Denis, G. Greig, S. Lamontagne, G. O'Neill, D. Slipetz, J. Wang, Benzimidazoles as new potent and selective DP antagonists for the treatment of allergic rhinitis, Bioorg. Med. Chem. Lett. 14 (12) (2004) 3195–3199.
[31] C. Kurz, I. Ungerer, U. Lipka, S. Kirr, T. Schutt, A. Eckert, K. Leuner, W.E. Muller, The metabolic enhancer piracetam ameliorates the impairment of mitochondrial function and neurite outgrowth induced by beta-amyloid peptide, Br. J. Pharmacol. 160 (2) (2010) 246–257.
[32] K. Leuner, C. Kurz, G. Guidetti, J.M. Orgogozo, W.E. Muller, Improved mitochondrial function in brain aging and Alzheimer disease - the new mechanism of action of the old metabolic enhancer piracetam, Front. Neurosci. 4 (2010).
[33] S.M. Cho, H.V. Kim, S. Lee, H.Y. Kim, W. Kim, T.S. Kim, D.J. Kim, Y. Kim, Correlations of amyloid-beta concentrations between CSF and plasma in acute Alzheimer mouse model, Sci. Rep. 4 (2014) 6777.
[34] M.S. Fanselow, A.M. Poulos, The neuroscience of mammalian associative learning, Annu. Rev. Psychol. 56 (2005) 207–234.
[35] Y.Z. Guo, R.C. Kalathur, Q. Liu, B. Kloss, R. Bruni, C. Ginter, E. Kloppmann, B. Rost, W.A. Hendrickson, Structure and activity of tryptophan-rich TSPO proteins, Science 347 (6221) (2015) 551–555.